Electroluminescence from ZnO Nanostructure Synthesizes between Nanogap

Cheng Jiang
Marquette University

ELECTROLUMINESCENCE FROM ZNO NANOSTRUCTURE SYNTHESIZED BETWEEN NANOGAP

by

Cheng Jiang

A Thesis submitted to the Faculty of the Graduate School,
Marquette University,
in Partial Fulfillment of the Requirements for
the Degree of Master of Science

Milwaukee, Wisconsin

December 2012

ABSTRACT
ELECTROLUMINESCENCE FROM ZNO NANOSTRUCTURE
SYNTHESIZED BETWEEN NANOGAP

Cheng Jiang

Marquette University, 2012

This thesis presents the investigation of a nanoscale light-emitting diode (LED) device. The nanoscale LED has a great potential to be used as a light source for biomedical screening and fluorescence lifetime spectroscopy. It can also be developed to a single photon emitter for the application of quantum computing.

The nano-LED has the electrical structure of a metal-semiconductor-metal (MSM) junction. The MSM junction has been formed on the nanogap device that is fabricated on a SOI wafer by optical lithography and KOH solution silicon etching. The Ni evaporated on the surface of the nanogap device performs the metal contact for the junction. The ZnO made by evaporation and thermal oxidation of Zn serves as the semiconductor part to realize efficient excitonic emission.

Photon emission phenomenon has been observed when bias is applied to the nano-LED device. The measured IV curve has confirmed the junction structure. The electroluminescence spectrum of the light has been obtained by using monochromator and CCD camera. The spectrum shows broad visual band wavelengths that are believed to result from some intrinsic defects of ZnO. The electroluminescence mechanisms are explained by the recombination of electrons and holes injected through thermionic emission, field emission, and thermionic-field emission.

ACKNOWLEDGMENTS

Cheng Jiang

I would like to express my gratitude to the people who gave me support during my thesis work.

First and foremost, I would like to express appreciation to my advisor, Dr. Chung Hoon Lee, for supervising this thesis and my two years' graduate research study. With his help, guidance, and encouragement, I acquired a lot of knowledge in the area of semiconductor devices and improved my ability to conduct scientific research.

I would like to thank Dr. Fabien Josse and Dr. Susan Schneider for being my committee members. They gave me many suggestions and comments to improve my research work in the past two years.

I would like to thank Jun Hyun Han, Robert Blise, and Michael Ziwisky for assisting me with device fabrication and instruments operation in the lab.

Finally, I am grateful to my parents. Without their support and encouragement, I would have never come to the United States to pursue my master's degree.

TABLE OF CONTENTS

LIST OF TABLES

LIST OF FIGURES

1 INTRODUCTION

The goal of this thesis is to investigate the properties and the light-emitting mechanisms of a nanoscale light-emitting diode (LED) device. The device has been fabricated on a silicon-on-insulator (SOI) wafer. A nanoscale gap has been formed by two silicon (Si) tips made on the top layer of the wafer. Nickel (Ni) has been evaporated on the tips and zinc oxide (ZnO) nanostructure has been synthesized between the nanogap. A metal-semiconductor-metal (MSM) junction is constructed by the Ni and ZnO. The device exhibits electroluminescence (EL) at moderate bias.

Nano-LEDs have a potential to be used as light sources for telecommunication, chip components communication, fluorescence lifetime spectroscopy, time correlated single photon counting, biomedical screening, and optoelectronic devices testing such as PMTs[1-5]. Nano-LEDs can also be developed to single photon emitters, which are essential components for optical quantum computing[1, 6].

Researchers have developed various methods to make nano-LEDs[7-16]. Many of these nanoscale light-emitting devices have the diode structures consisting of semiconductors such as ZnO, gallium nitride (GaN), gallium arsenide (GaAs), and indium arsenide (InAs). The diodes are based on some nanoscale structures like quantum dots, nanowires, or nanorods. Various materials have been used as the substrate for the diodes[7-16]. Nadarajah et al have grown ZnO nanowires to form the LED on an indium tin oxide coated polyethylene terephthalate foil[9]. Chen et al have fabricated an n-p-n junction based on ZnO nanowires with an ITO/glass substrate underneath[10]. Tan et al have designed a CdS/ZnS quantum dots LED on top of a glass substrate[11]. Kwak et al have made quantum dot LEDs using a multilayer structure consists of aluminum (Al),

molybdenum trioxide, colloidal quantum dots, ZnO, and indium tin oxide[12]. However, since silicon is the predominant material of present electronic technology, it is more convenient to use silicon as the substrate because glass, polymer or complex multiplayer structures require hybridization with the silicon based circuitry. To grow II-VI or III-V compound semiconductors on silicon substrate may be a simple and direct method to integrate optoelectronics and CMOS circuits[8]. In addition, nanowire LEDs have the issues of poor crystalline quality and random entangle structures, which may limit the usage of the devices in practical applications[16]. Plenty of nanoscale LEDs are designed to emit light at specific frequency or show a narrow emission band around certain wavelengths[7-8, 11-12], whereas broad visible band light sources can be useful as well and may have applications not obtainable by single wavelength light sources such as visible light communication[17-18]. A large amount of nanoscale light-emitting devices or single photon sources require optical excitation. Compared with optically driven devices, electrically driven light sources may be more suitable for chip-scale electronic circuit application.

Our nano-LED devices have several advantages. The ZnO nanostructure is formed by thermal oxidation of evaporated Zn at 350 ℃, which is a lower temperature than the CMOS thermal budget of 400-450 ℃[8]. The diode structure and electrical contact are monolithically integrated on a single silicon substrate, facilitating CMOS compatibility. The electroluminescence spectrum is in the visible band ranging from 450 nm to 1000 nm and photons of different frequencies can be filtered for various applications. For a better understanding the characteristics of the device and exploring

potential applications, the electrical and optical properties of the nano-LED have been tested and the principles of the light emission phenomenon has been analyzed.

1.1 Nanotechnology

The development of nano-LED devices belongs to the field of nanotechnology.

Nanotechnology is defined as the design, fabrication and application of materials, devices and systems with control at nanometer dimensions[19]. In the past few decades, nanotechnology has been playing an important role in various scientific areas.

Currently, the research in the field of nanotechnology has three main directions: nanoscale science, nano-materials development, and modeling. At the nanometer level, both classical mechanics and quantum mechanics operate on objects. Exploring the laws of physics at the nanoscale can help us understand the interactions of the objects. The investigation of the formation and properties of nanoscale materials is also of great significance. Many materials exhibit different structures and characteristics at the atomic level. The research in this aspect will give us a good idea of how these materials can be used in devices and systems to achieve unique functions that may not be realized by the materials in the bulk form. The modeling of the nanoscale materials, devices, and interactions is essential for nanotechnology as well. It can be used in predicting the behavior of the atoms in the nanoscale systems[20].

There are many advantages that we can benefit from nanotechnology. Firstly, for nanoscale materials, the surface-to-volume ratio is greatly increased because many of the atoms stay on the materials' surface. The larger surface-to-volume ratio results in a dramatic improvement in the properties of the materials and devices whose performance

rely on specific surface area. Secondly, the miniaturization of the materials may bring a better change in the intrinsic properties of the materials. When the device is small enough, the energy levels become discrete, which allows the output energy to be adjusted according to the size of the material, especially for some electronic and photonic devices. Finally, the combination of diverse properties of different materials into one material could be achieved at the nanoscale level[19].

Nanotechnology has showed great impact in different industries that include electronics, optics, biomedical engineering, and so forth[19-52].

The most widespread application of nanotechnology in electronics is circuit miniaturization[19]. At present, microelectronics is recognized as a key technology for information systems. Electronic components and systems are downsized to micrometer dimensions. A wide variety of micro-electro-mechanical system (MEMS) products, such as accelerometers, gyroscopes, pressure sensors, and micromirrors, are utilized in a broad range of applications. The progress in microelectronics has indicated that the reducing of dimensions could bring faster, more powerful, more reliable and less expensive electronic circuits. The growing demands of more powerful integrated circuits for information technology lead to the transition to nanoelectronics[21]. At the same time, microscale electrical systems can perform as a platform for the integration of nanotechnology so that nanoscale systems can interact with the macroscale world[22]. A main class of nanoelectronic devices is solid-state quantum effect devices. These devices usually rely on certain solid-state nanostructures such as nanotubes, nanowires, quantum wells, and quantum dots[23]. Research groups have reported using carbon nanotubes to achieve field-effect transistors[24], single-electron transistors[25], logic circuits[26], and memory storage

elements[27]. Nanowires, usually grown from semiconductors like silicon, silicon germanium, GaAs, gallium phosphide (GaP), InAs, and indium phosphide (InP) or metal like gold, silver, and copper, are considered as building blocks for nanoelectronic devices[1]. Recent research has demonstrated that nanowires are good candidates for making field effect transistors[28], light-emitting diodes[9, 10], resonators[29], and nanomagnets[30]. Researchers have also been working on controlling the growth of the nanowires to make diodes and transistors and on integrating arrays of nanowires to form microelectronic circuits [31-33]. Quantum dots with controllable electron spins are believed to be a promising method for realizing quantum computing[34].

In optics, the wavelength of light is in the nanometer domain. Optical studies in which light is confined and modulated in structures smaller than the wavelength are considered to be nanoscale science. The behaviors and properties of the particles or patterns in the wavelength size are often dominated by geometric parameters. Nanotechnology may revolutionize optics, photonics, and lighting and color technology[35]. A well-known application of nanotechnology in optics is fiber-optic communication, which is the method of transmitting information between two places by sending pulses of light through an optical fiber[36]. Two cardinal developments for the achievement of fiber-optic communication are quantum well lasers based on InP that operate in single longitude mode and erbium doped fiber amplifiers and nanoscale fiber gratings that provide uniform amplifications[37]. Nowadays it is largely used to transmit telephone signal, Internet communication and television signals by many telecommunications due to its advantages of high data transmission rates and lower interference and attenuation for long distance communication compared with conventional copper wire[38]. New classes

of optical sources, guides and detectors based on semiconductor nanostructures have started to emerge. The quantum well lasers available in the market have the advantages of high temperature stability, good coherency, and low threshold current[23]. Researchers have also developed quantum dot lasers and quantum dot light detectors by means of assembling InGaAs quantum dots on GaAs substrates[39, 40]. The large optical gain of quantum dots results in lower threshold current densities and higher frequency limits for modulation[23]. Additionally, the emission wavelength from nanocrystals can be precisely tuned because the values of energy levels have direct relation to the size of the nanoparticle. Based on this property, new type of quantum dots fluorescence emitters has been developed. The characteristics of tunable spectral range, large absorption coefficients, and high levels of brightness and photostability make quantum dots emitters particularly attractive for the applications in live cell imaging, tissue labeling, and live animal imaging and targeting[41]. A lot of research studies are aimed at making minuscule light-emitting devices and such devices are of great use in telecommunications. Researchers have shown that they use nanotubes to emit 1.5 micron infrared light and this wavelength is widely used in long-distance telecommunication. Another research group has found a way to make light-emitting diodes by crossing two types of nanowires and the emitted light is in the red and infrared ranges[1]. Tiny light-emitting diodes can be used to develop single photon sources as well. Of many physical implementations of quantum bits, single photons are considered to be a leading approach because they are less disturbed by noise and have the ability to be encoded in several degrees of freedom in polarization, time bin and path[6]. In 2001, Knill et al showed that quantum gates and optical circuits could be realized by using wave plate and beam splitters, which made

using only beam splitters, phase shifters single photon sources and detectors to achieve quantum computing possible[42]. As a result, single photon sources are a key component of quantum computing and quantum cryptography.

Biomedical nanotechnology has led to advances in diagnostic techniques[43]. For example, quantum dots can be conjugated to biological molecules like proteins or peptides by some approaches, such as adsorption, electrostatic interaction, and covalent linkage without disturbing the biological function. These quantum dots will emit light after being excited, which can be used as biomarkers for detecting and labeling of molecules, cells or tissues. The detection sensitivity can be further improved by measuring the Stoke shifts, that is, the distance between the excitation and emission peaks, of the quantum dots[41].

With the development of nanotechnology, the size of the existing materials and devices can be reduced and the performance could be vastly enhanced. New type of devices and systems can be created, which may open up novel areas of applications.

1.2 LED

In this thesis, nanotechnology has been employed to develop a light-emitting diode. Basic knowledge about light-emitting diodes is introduced here.

Light-emitting diodes are the devices that convert electrical energy into optical radiation. As important semiconductor light source, LEDs have found widespread use in myriad areas in our daily lives as well as scientific fields like communication and medicine[44].

LEDs belong to the luminescent device family. Luminescence is the emission of optical radiation resulting from electronic excitation in a material[44]. There are three main optical processes for interaction between a photon and an electron in a solid: absorption, spontaneous emission, and stimulated emission. Of these three, spontaneous emission, in which a photon is emitted when the electron in the conduction band spontaneously returns to the empty state in the valence band, is the main process that happens in LEDs. Luminescence can be divided into four types by the source of the input energy: photoluminescence (PL) that is excited by optical radiation, cathodoluminescence (CL) that is excited by electron beam or cathode ray, electroluminescence that is excited by current or electric field, and radioluminescence that is excited by other fast particles or high-energy radiation[44]. LEDs are injection electroluminescent devices. The emission of radiation results from the combination of the minority carriers injected by the electric current with majority carriers[45]. More details about electroluminescence will be discussed later in chapter 4.

A LED is a semiconductor *p*-*n* junction. When the junction is forward biased, minority carriers will be injected to the junction from both sides. Recombination will take place at the vicinity of the junction with the release of photons[44]. The ideal current-voltage (I-V) characteristic of a p-n junction follows the equation:

$$I = I_0(e^{qV/kT} - 1), \tag{1.1}$$

where q is electron charge, k is Boltzmann's constant, V is bias voltage, T is temperature, and I_0 is reverse saturation current[45]. The energy of photons emitted from the semiconductor is approximately equal to the bandgap energy E_g, i.e.

$$E_g \approx h\nu, \tag{1.2}$$

where h is the Planks' constant, v is the frequency of the photon[46]. The conservation of energy requires the energy of the injected electron is equal to the photon energy. So, the diode voltage V_d can be given by:

$$V_d = \frac{h\nu}{e} \approx \frac{E_g}{e} . \tag{1.3}$$

The emission corresponding closely in energy to bandgap is just one type of recombination transitions. There are also transitions involving chemical impurities or physical defects, in which the energy of the emitted light is smaller than the bandgap energy[44]. More details about defect related transitions will be discussed later in chapter 5.

LEDs are often made from inorganic semiconductor materials include aluminum gallium arsenide, GaP, gallium arsenide phosphide, zinc selenide, and indium gallium nitride[47]. Some organic compounds can be used to develop organic LEDs, for example, molecules of tris(8-hydroxyquinolinato)aluminium, polymers of poly(*p*-phenylene vinylene), and some phosphorescent materials[48-50].

The LEDs available on the market have plenty of color options ranging from ultraviolet to infrared. The lights of different colors are related to different wavelengths. White LEDs with broad spectra have also been developed.

The applications of LEDs can be categorized into three kinds. The first application is for illumination. LEDs have the advantages of high efficiency, higher reliability and longer lifetime over traditional incandescent light bulbs. Another application is for displays in electronic equipment and outdoor indicators. The third application is as light source for communication. GaAs LEDs can be applied in free-space communication, such as remote control of appliances like television sets and

stereos. Infrared LEDs are also good light sources for local area optical-fiber communication for low and medium bit rate[44, 51].

The progress in the area of light-emitting diodes has been breathtaking. The technology developed for LEDs enables the creation and improvement of nanoscale LEDs. As mentioned earlier, nanoscale LEDs based on quantum dots can offer size- and composition-tunable emission wavelengths. Nano-LEDs have the ability to be attached to biomolecules as well and the molecules can be detected by measuring the shifts of the wavelength before and after conjugation. The nano-LEDs with wide spectral range are appealing for multiple parameters imaging or tracking in biological and medical applications[41]. Nano-LEDs can be developed to generate single photons. The number of the photons emitted from faint laser pulses obeys Poissonian statistics[52]. True single photon sources could be realized by nano-LEDs, which are ideal light sources for quantum information and time correlated single photon counting[5-6]. Nano-LEDs can produce reliable nanosecond optical pulses, which are of great use in fluorescence lifetime spectroscopy[53-54]. The development of nano-LED devices is very necessary because of these useful and promising applications.

1.3 ZnO as a Light-emitting Semiconductor

Many wide bandgap semiconductors such as silicon carbide (SiC), GaN, GaAs, and ZnO have been studied for LEDs or other optoelectronic applications. SiC has been used in LEDs for blue and ultraviolet light generation for a long time. But due to the unfavorable indirect bandgap of SiC, the efficiencies are very limited. SiC can no longer compete with III-V semiconductors like GaN and GaAs[55]. GaAs is a popular direct

bandgap material for light-emitting applications. Infrared LEDs and lasers based on GaAs have been reported[51]. However, GaAs has several drawbacks. GaAs is rare and hard to obtain. Arsenic is toxic, which may cause problems during handling and disposal processes of the material[56]. Electronic devices based on GaAs cannot tolerate elevated temperatures or chemically hostile environments[55]. GaN is also a direct bandgap semiconductor and it is well known for the high efficiency. GaN can be operated as emitters and detectors in the blue-green, blue and ultraviolet region of the optical spectrum[55]. However, GaN is a relatively expensive material. Growing GaN in bulk is difficult and time-consuming. Exceedingly high concentration of extended defects may be produced because of the lattice mismatch between GaN and the sapphire substrate[57]. ZnO has been proposed as a promising material to substitute GaN. The most obvious key fact for using ZnO is that it is intrinsically inexpensive, easy to access, safe and stable[58]. ZnO is a wide and direct bandgap semiconducting material with E_g=3.3 eV at room temperature. The large bandgap brings ZnO the advantages of high breakdown voltages, lower noise and the ability to be operated under large electric field and high temperature[59]. ZnO has high exciton binding energy of 60 meV, which ensures efficient excitonic emission at room temperature[60]. The high electronic energy of band-to-band transitions allows emission in the green, blue and UV spectra. Functional oxides of wide bandgap semiconductors like ZnO can arrange to form novel nanostructures such as nanowires, nanotubes, nanorods, which are the fundamental building blocks of small and smart devices. ZnO is also a bio-safe and biocompatible material that can be used for biomedical applications. In addition, as an important piezoelectric material, ZnO attracts great attention for the applications of piezoelectric transducers, varistors, surface acoustic

wave devices, and so on[58-63]. These favorable features of ZnO drive us to choose ZnO as the semiconductor material for our nano LED devices.

ZnO is a II-VI compound semiconductor. The ionicity of ZnO is between ionic and covalent semiconductors. ZnO has three crystal structures: wurtzite, zinc blende and rocksalt. Zinc blende structure can only be stably grown on cubit substrates and rocksalt structure may be obtained under high pressure. Normally, ZnO forms in the wurtzite crystal structure under ambient conditions due to some intrinsic or extrinsic defects such as Zn interstitial and O vacancy, but the subject is still under debate[59]. As shown in Figure 1-3-1, wurtzite ZnO has a hexagonal unit cell with lattice parameters *a*=3.25 Å and *c*=5.2 Å. The wurtzite structure has alternating planes consisting of tetrahedrally coordinated Zn^{2+} and O^{2-} ions that are stacked alternatively along the *c* axis. The tetrahedral coordination causes a non-central symmetric structure[59].

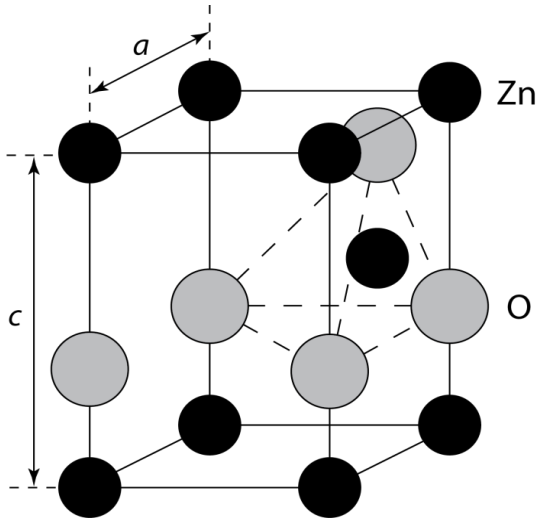

Figure 1-3-1. Wurtzite ZnO structure.

ZnO is a relatively soft material. The approximate hardness of ZnO on the Mohs scale is 4.5. The elastic and bulk moduli of ZnO are small. Experiments have shown that ZnO becomes softer against shear-type distortions. ZnO exhibits plastic deformation when relatively low loads are applied. The Young's modulus of ZnO remains essentially constant with $E = 111.2 \pm 4.7$ GPa. The non-central symmetric structure also results in piezoelectricity, pyroelectricity and spontaneous polarization along the *c*-direction[59].

Some basic physical properties of ZnO have been shown in Table 1-3-1[63].

Table 1-3-1. Properties of wurtzite ZnO.

Properties	Value
Lattice parameters at 300 K	
a_0	0.32469 nm
c_0	0.52069
Density	5.606 g/cm^3
Melting point	2248 K
Relative dielectric constant	8.66
Gap Energy	3.3 eV
Exciton binding energy	60 meV
Electron effective mass	0.24
Electron mobility (T = 300 K)	200 cm^2/V s
Hole effective mass	0.59
Hole mobility (T= 300 K)	5-50 cm^2/V s

Different techniques can be used to achieve the growth of ZnO nanostructures, such as metal organic chemical vapor deposition (MOCVD), vapor liquid solid (VLS), aqueous chemical growth (ACG), thermal oxidation, sputtering, molecular beam epitaxy (MBE), pulsed laser deposition, and so forth[64-71].

The studies of the optical properties of ZnO are conducted by various methods based on different luminescence mechanisms that are photoluminescence,

electroluminescence, and cathodoluminescence. The spectra obtained from ZnO vary when the growing and measuring methods are different[64-71]. The ZnO spectra will be further discussed in chapter 5.

1.4 Thesis Outline

The content of this thesis is organized in the following way. Chapter 1 introduces the object and the background of the thesis. Chapter 2 describes the design and fabrication of the nano-LEDs. Chapter 3 presents the setup and the results of the experiments for testing properties of the nano-LEDs. Chapter 4 discusses the analysis of the electron transport mechanisms in metal-semiconductor junctions. Chapter 5 presents the electroluminescence mechanism in nano-LEDs and the source of the ZnO spectrum. At last, chapter 6 summarizes the work and chapter 7 gives suggestions for future work.

2 NANO-LED DEVICE FABRICATION

The fabrication process of the nano-LED devices is explained in this chapter. The process includes making nanogap devices and growing ZnO nanostructures between the nanogaps. Sharp tips are formed on the top silicon layer of the wafer by wet chemical etching. The silicon tips are then suspended by removing the SiO_2 underneath. The tips are covered with Ni after evaporation and Ni acts as the electrical contact for the nano-LED. The nanogap between the tips is filled with Zn after another evaporation process. The Zn is converted to ZnO by thermal oxidation, which is the semiconductor part of the nano-LED for emitting light.

2.1 Fabrication of Nanogap Devices

The nanogap devices are fabricated on a SOI wafer by optical lithography and anisotropic wet chemical silicon etching with a unique double-layer etch mask[72].

The substrate of the SOI wafer consists of a layer of Si with the thickness of 3 μm on the top, a layer of silicon dioxide (SiO_2) with the thickness of 5 μm in the middle and a bottom layer of Si with the thickness of 500 μm. Before fabrication, a thermally grown SiO_2 film with the thickness of 0.27 μm and a low stress LPCVD silicon nitride (SiN) film with the thickness of 0.5 μm are deposited on the substrate. The SiN and SiO_2 films are used as masks for potassium hydroxide (KOH) etching. The structure of the substrate before fabrication is shown in Figure 2-1-1.

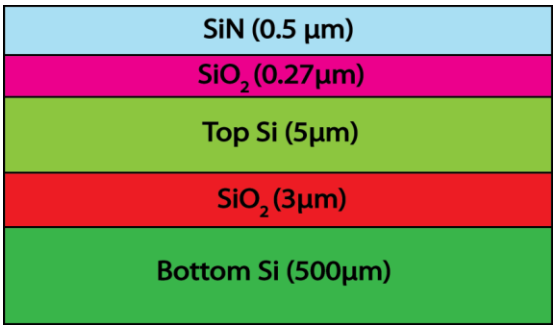

Figure 2-1-1. Wafer structure before fabrication.

The overall fabrication process includes three times of optical lithography, with the first one for SiN etching and the following two for Si etching.

To begin the lithography, the wafer is cleaned using piranha (H_2SO_4 and H_2O_2) solution and dehydrated on the hot plate at 300 ℃ for five minutes. Hexamethyldisilazane (HMDS) vapors are applied to the wafer surface to enhance the adhesion of photoresist (PR). The wafer is then coated with a layer of photoresist and soft baked on the hot plate at 110 ℃ for one minute. After being exposed to UV light for 12 seconds with the first layer of the etch mask aligned on the top, the wafer is put into the developer to dissolve the exposed part. The remaining photoresist functions as the mask for the SiN etching using tetrafluoromethane (CF_4) plasma in a vacuum chamber for 20 minutes. Figure 2-1-2 shows the top view of the device after the first lithography.

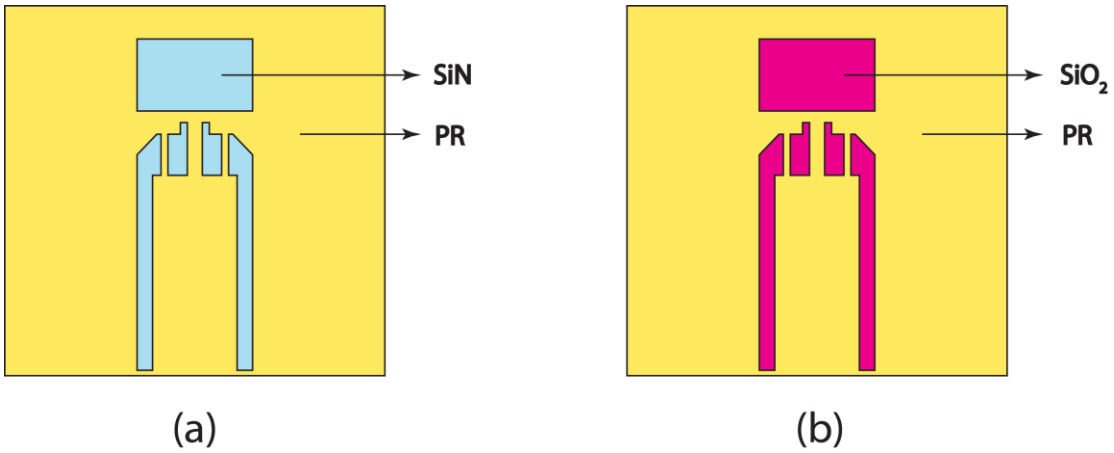

Figure 2-1-2. Top view of the device after the first lithography: (a) before SiN etching; (b) after SiN etching.

Another lithography process is conducted for the first step of Si etching. After being coated with photoresist and soft baked at 110 ℃ for one minute, the wafer is aligned under the second layer of the etch mask and exposed to UV light for 8 seconds. The second time of baking is conducted at 130 ℃ for two minutes. The wafer is then exposed to UV light without the etch mask for 30 seconds. After developing, the remaining photoresist has the pattern of the inverse image of the etch mask. The exposed portion of the SiO_2 is removed with buffered oxide etch (BOE) solution. The underlying Si is etched by KOH solution. The KOH solution has the concentration of 30% and the etch rate is 0.31μm per minute at 60 ℃. Figure 2-1-3 shows the structure of the device after the second lithography. The KOH solution keeps etching the Si layer until the width of the Si cantilever beam in the middle of the top Si layer is about 2.5 to 3μm. A thermal oxidation process is conducted and a layer of SiO_2 is formed on the surface of the exposed part of the Si layer in order to prevent the Si from being further etched in the second KOH etching.

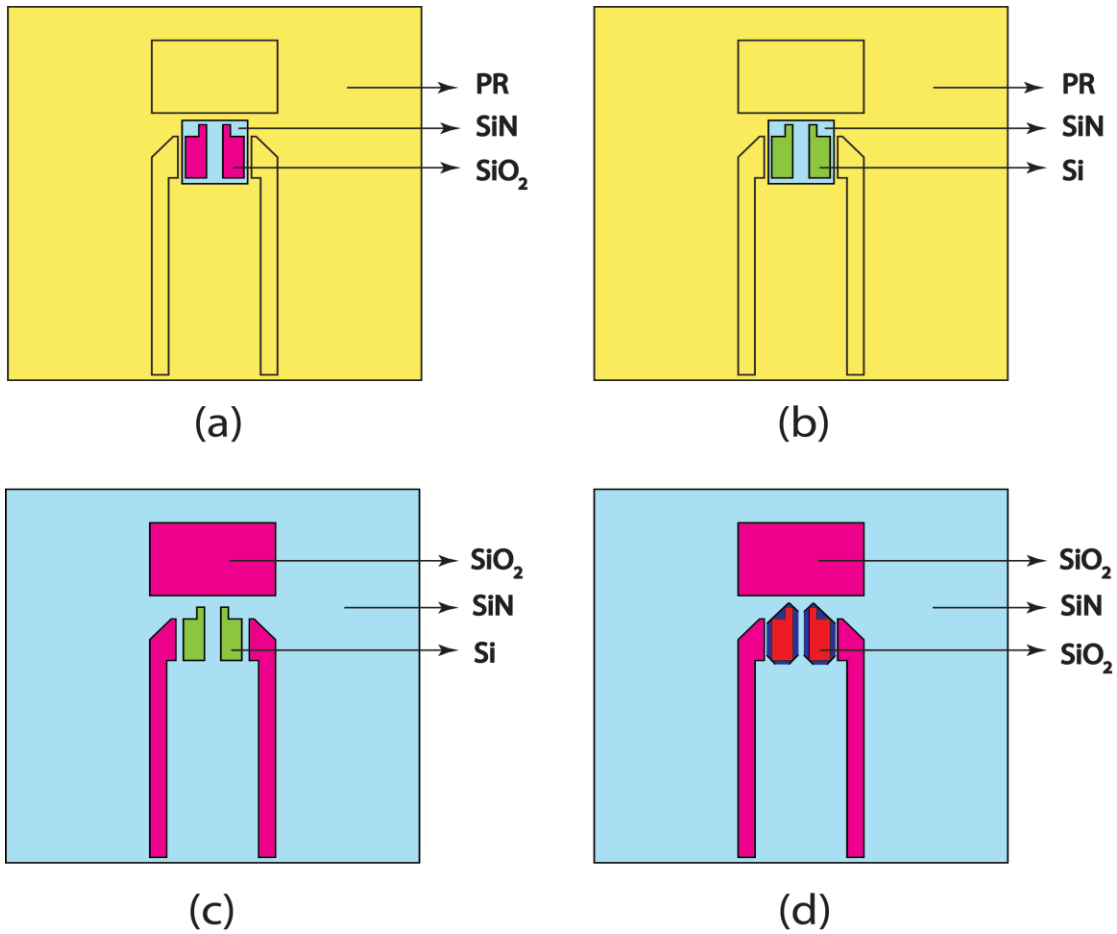

Figure 2-1-3. Top view of the device after the second lithography: (a) before SiO_2 etching; (b) after SiO_2 etching; (c) after removing photoresist; (d) after Si etching with KOH solution.

The next step of fabrication is the third lithography. The processes of wafer cleaning, photoresist coating and soft baking are similar as those in the first lithography. The second layer of the etch mask is used during the exposure to the UV light for 20 seconds. After being developed, the remaining photoresist has the exact copy of the pattern on the etch mask. The uncovered SiO_2 is etched using BOE solution and the Si underneath is etched by KOH solution for about 1 hour. After etching, the surface layer of the bare Si is converted to SiO_2 by another oxidation process. The purpose of the oxidation is to protect the Si from being etched during the following SiN etching. Then

the SiN layer is removed by phosphoric acid. The SiO_2 layer under the SiN and the uncovered portion of the SiO_2 on top of the bottom Si are both removed by BOE solution. Figure 2-1-4 shows the structure of the device after the third lithography.

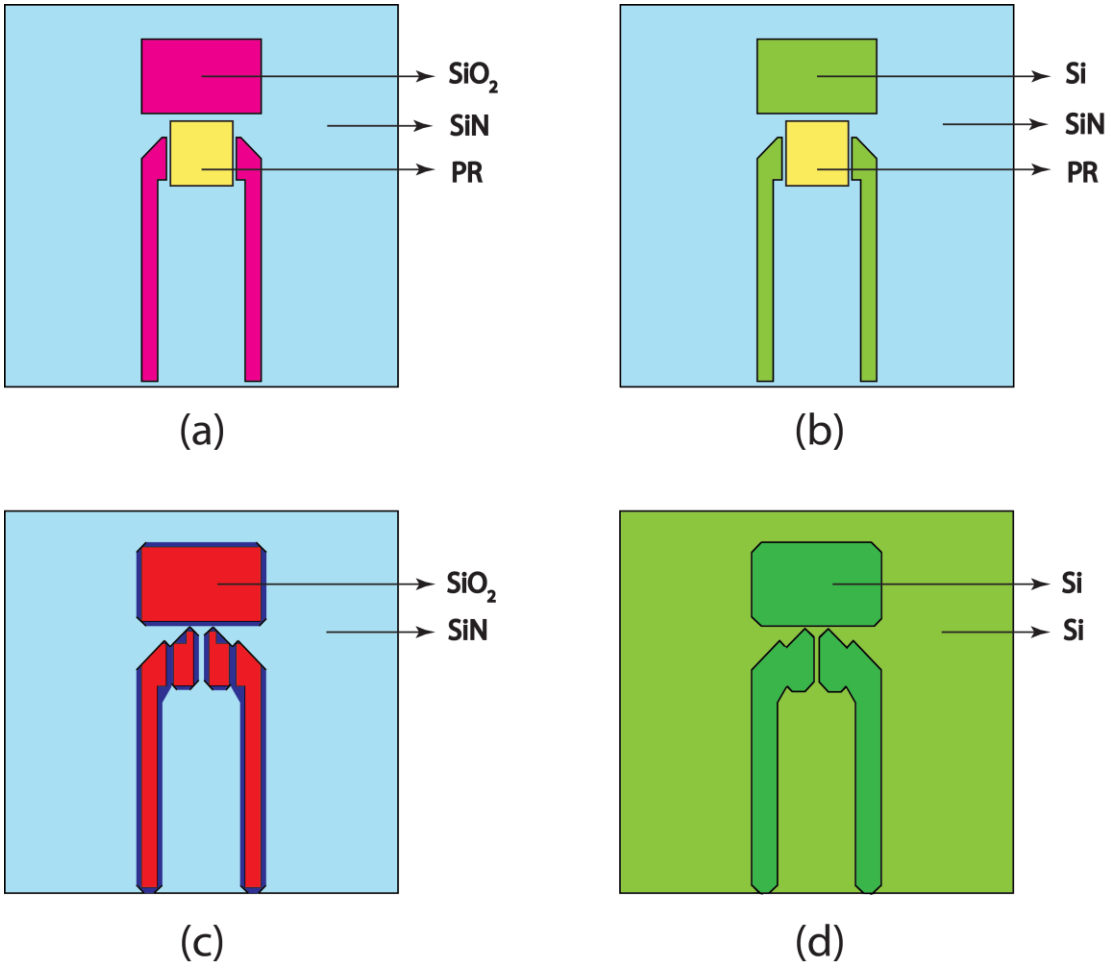

Figure 2-1-4. Top view of the device after the third lithography: (a) before SiO_2 etching; (b) after SiO_2 etching; (c) after removing photoresist and Si etching with KOH solution; (d) after removing SiN and SiO_2.

The nanogap device is shown in Figure 2-1-5. As can be seen in the figure, sharp tips are fabricated on the top Si layer of the device. The tips are formed by the (111) silicon crystal plane created during the first KOH etching and (100) plane created during

the second KOH etching. There are nanoscale gaps between the sharp tips and the average size of the gaps is a few tens of nanometers.

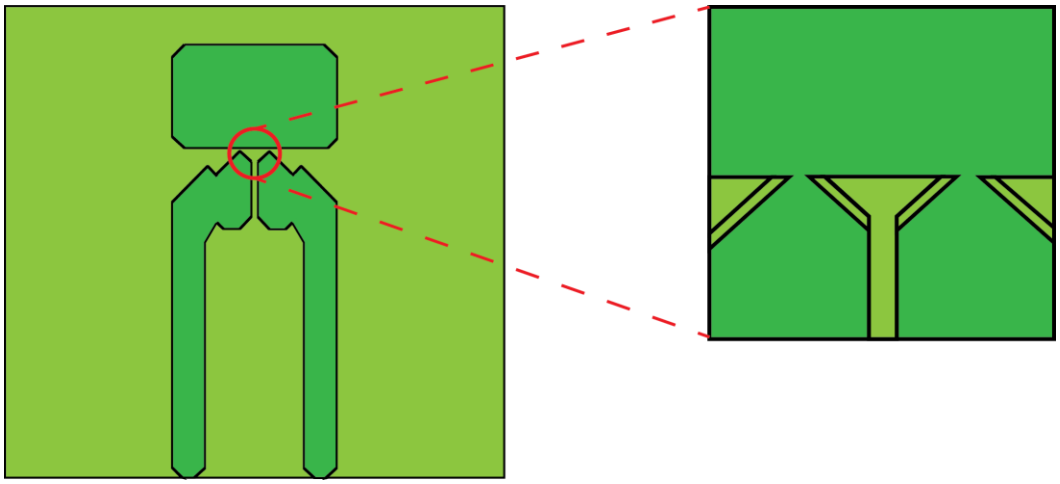

Figure 2-1-5. Top view of the S1 nanogap device and close up view of the nanogap.

Four different designs of nanogap devices are fabricated together on one wafer. The configuration shown in Figure 2-1-5 is named as S1 device. Figure 2-1-6 shows the configuration of the S2 nanogap device.

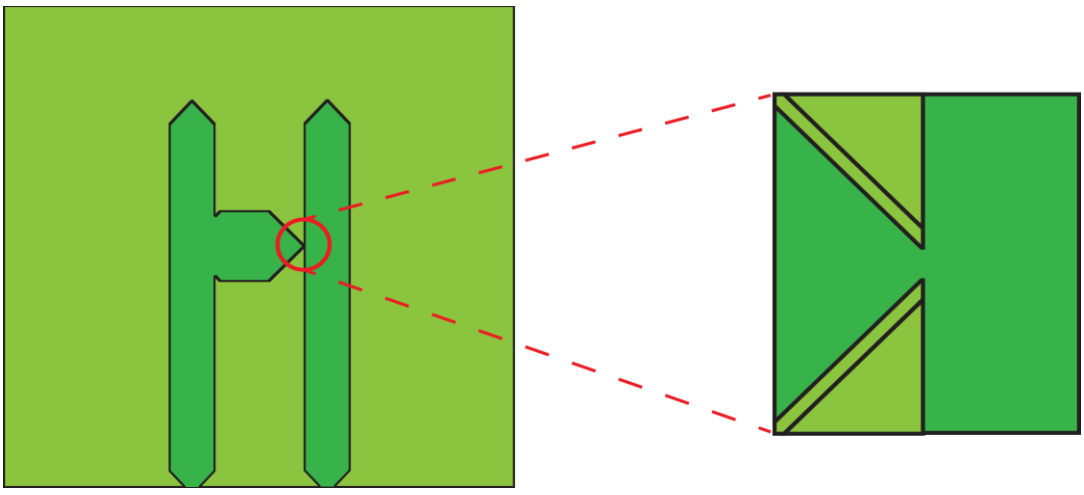

Figure 2-1-6. Top view of the S2 nanogap device and the close up view of the nanogap.

The size of the nanogap can be estimated using Simmon's Model. A MATLAB program has been made to calculate the gap size. Details about the Simmon's Model and the program are in the appendix.

2.2 Growth of ZnO Nanostructures between Nanogaps

ZnO nanostructures are synthesized between the nanogaps by thermal evaporation of Ni and Zn and thermal oxidation of Zn.

After making nanogap devices, a layer of Ni with the thickness of 30 nm and a layer of Zn with the thickness of 50 nm are thermally evaporated on the devices in a vacuum of ~10^{-7}Torr. After that, the Zn film on the devices is oxidized to ZnO film at 350 ℃ in a quartz tube furnace with an oxygen flow of 5 sccm (Figure 2-2-1). Figure 2-2-2 shows the cross-sectional view of the device before and after the metal evaporation and the Zn oxidation.

Figure 2-2-1. Lindberg/Blue M quartz tube furnace.

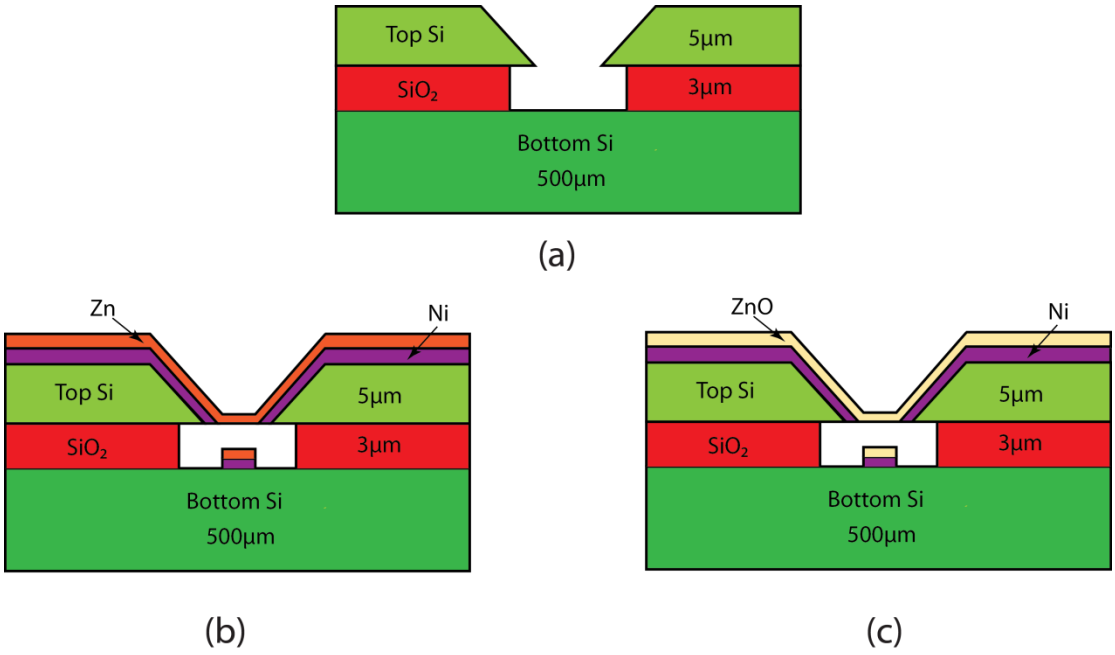

Figure 2-2-2. Cross-sectional view of the device: (a) nanogap device; (b) device after evaporation of Ni and Zn; (c) device after Zn oxidation.

Different kinds of metals have been considered as the electrode material for the nano-LED devices. However, alloy may be formed between Zn and other metals like aluminum and copper during the thermal oxidation process because of the high temperature. Compared with them, Ni reacts less with Zn at elevated temperature. As a result, Ni is preferred to perform the electrical contact for our device.

The images of the nanogap taken by scanning electron microscope (SEM) are shown in Figure 2-2-3.

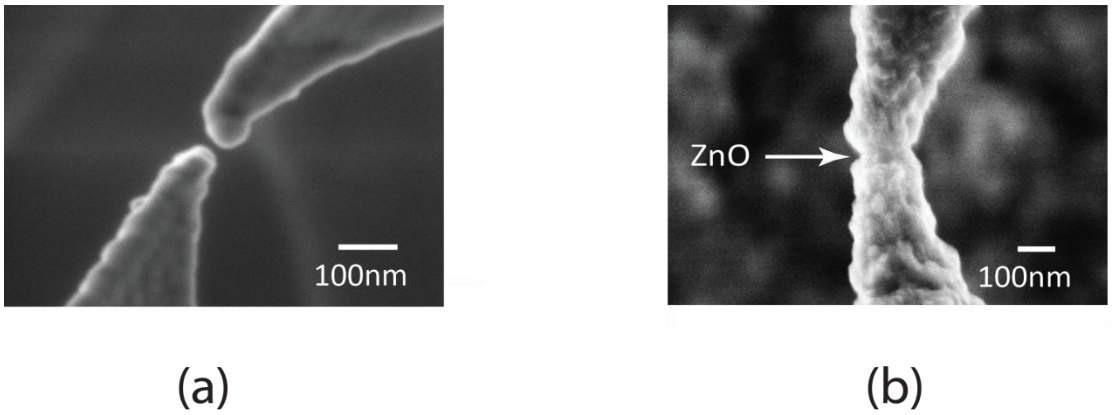

Figure 2-2-3. SEM images of the nanogap: (a) close-up view of the gap;
(b) after evaporation and oxidation.

As can be seen in the picture, the nanogap is filled with ZnO after the evaporation of Ni and Zn and the Zn oxidation.

3 EXPERIMENT METHODS AND RESULTS

To investigate the nano-LED, the electrical properties and optical properties of the devices have been tested. Emission of light has been observed from the ZnO nanostructure when bias is applied to the nano-LED device. The Current-Voltage characteristics of the nano-LED have been tested. The spectrum of the light has been measured in order to analyze the source of emitted light. The intensity of the light with respect to different voltage levels has been measured as well, which proves that the nano-LED device can possibly be used as a single photon source. In this chapter, the details of the experiment methods will be presented and the results of the experiments will be shown.

3.1 Electroluminescence from Nano-LED

As a light source, the nano-LED is electrically biased for the light-emitting test.

To test the electroluminescence (EL) from the nano-LED, a Keithley 2400 Source Meter is used to apply current to the device. On the device, the Ni layer serves as the electrodes to the ZnO nanostructure between the nanogap. Two probes connected to the Keithley land on the two sides of the nanogap and the current passes the ZnO nanostructure through the Ni electrodes. Figure 3-1-1 is the picture of a S2 nanogap device under test taken by an optical microscope that has the magnification of 100. The cross-sectional view of the device under test is shown in Figure 3-1-2.

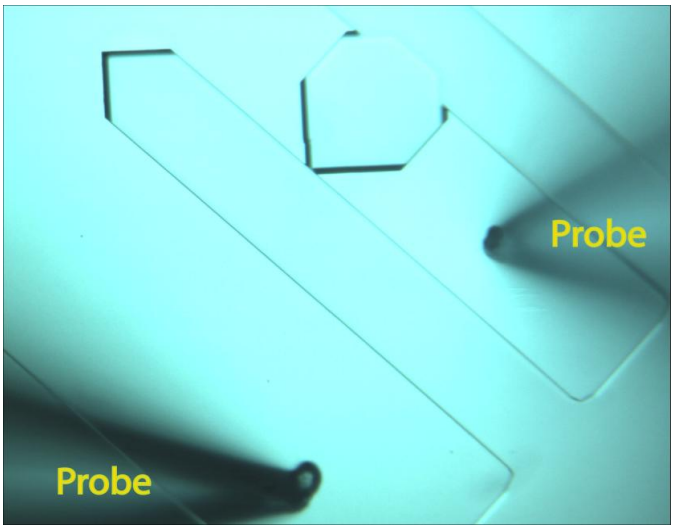

Figure 3-1-1. Device under test under optical microscope.

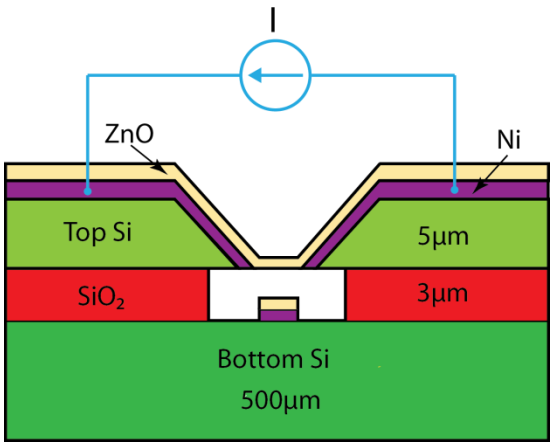

Figure 3-1-2. Cross-sectional view of the device under test.

When the device is under bias, high electric field exists between the tips and carrier transport will happen at the metal-semiconductor interface. Only the ZnO nanostructure between the nanogap is electrically active and electroluminescence may happen from the nanostructure.

The result of the electroluminescence test is shown in Figure 3-1-3.

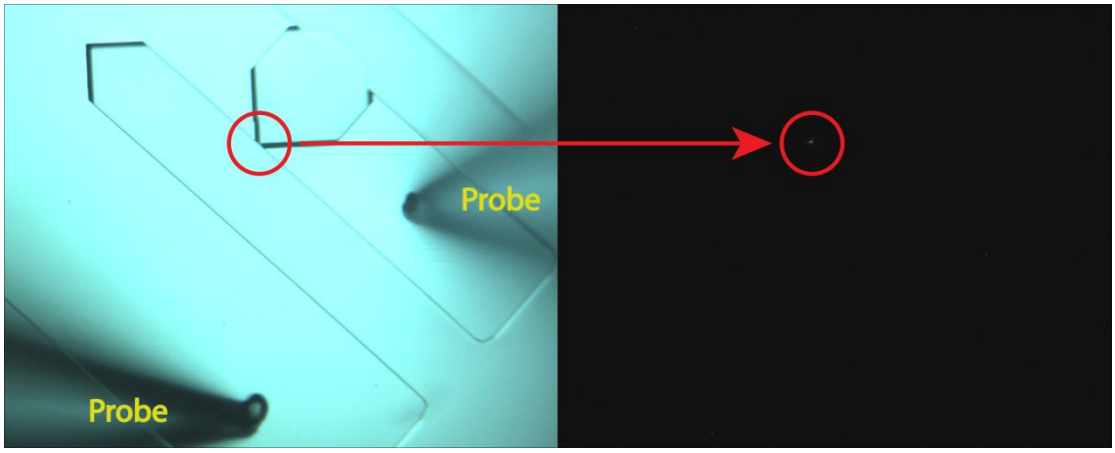

Figure 3-1-3. Electroluminescence of the ZnO nanostructure between the nanogap.

In the test, the Keithley provides a current of 10μA to the ZnO nanostructure through the probes. When light of the microscope is turned off, emission of light is observed right from the position of the nanogap, which proves the happening of electroluminescence of the ZnO nanostructure between the gap.

3.2 Spectrum of the Light Emitted from Nano-LED

ZnO is a II-VI direct bandgap semiconductor[59]. The emission spectra of ZnO strongly depend on the preparation methods and the growth conditions. In this research, the X-ray diffraction (XRD) data (Figure 3-2-1) of the oxidized Zn film has shown that the ZnO prepared by thermal oxidation of Zn possesses polycrystalline wurtzite crystal structure. However, since the width of the gap is only several tens of nanometers, the size of the synthesized ZnO nanostructure could be smaller than the mean grain size of the polycrystalline ZnO film. The ZnO nanostructure may have the structure of single crystal, which allows radiative recombination to occur in the direct bandgap. Thus the

electroluminescence could be explained. To find out the source of the photon emission, the spectrum of the light has been measured.

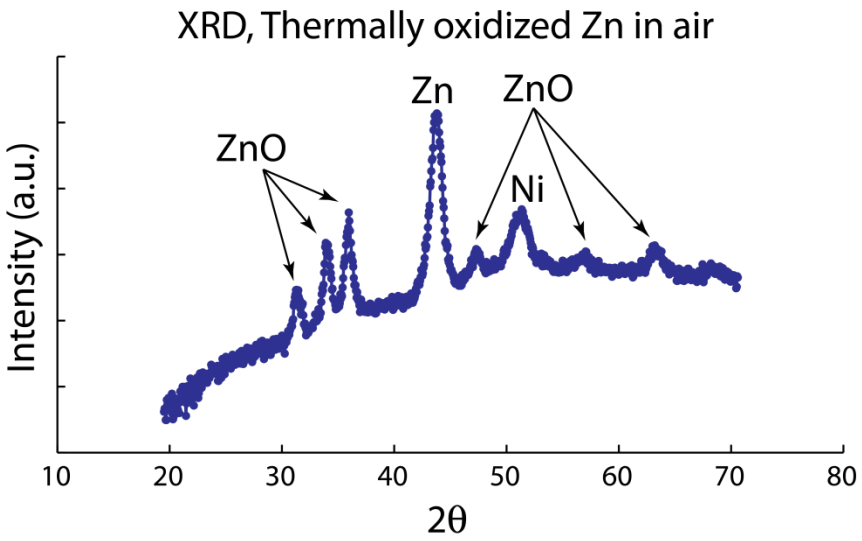

Figure 3-2-1. X-ray diffraction data of the thermally oxidized Zn film.

An Acton MicroSpec 2300i monochromator with a Princeton Instruments Cascade 512B (CCD 97) camera is used to get the spectrum of the light emitted from the nano-LED.

The working principle of the monochromator is explained in Figure 3-2-2. A polychromatic light is aimed at the entrance slit of the monochromator. When the light encounters the grating inside, it is dispersed and different wavelengths will reflect at different angles. The grating rotates slowly and the dispersed light is reimaged so that each wavelength could be directed to the exit slit and detected by the CCD camera. By comparing the intensity of the light of different wavelengths, the spectrum can be obtained.

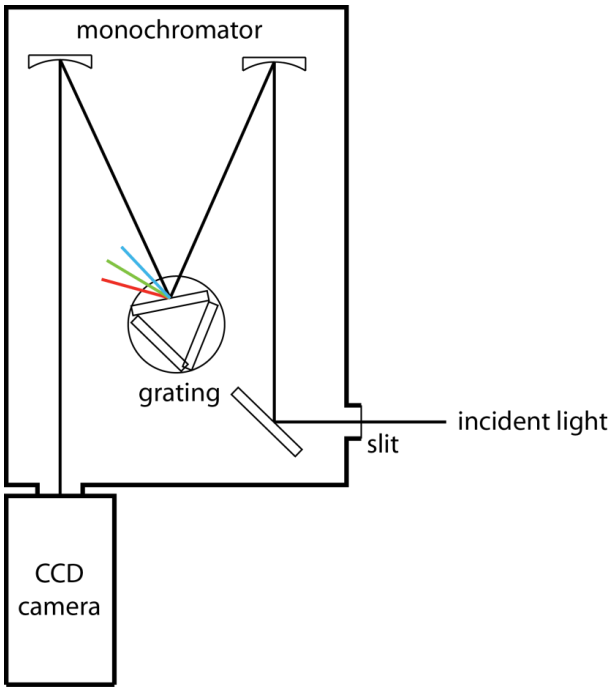

Figure 3-2-2. Working principle of monochromator.

The setup of the experiment is shown in Figure 3-2-3. The sample devices are bonded on an acrylic plate that has two testing probes mounted on it. After adjusting the position of the probes under optical microscope, the plate is mounted on an optical stage. The stage can be moved back and forth to adjust the focus of the image to the camera. The device can be located on the screen by moving the stage left and right. The stage with the sample on it is then put into a big box that is covered with aluminum foil (Figure 3-2-3 (a)). The probes are connected to the Keithley outside the box through wires (Figure 3-2-3 (c)). A lens with the magnification of 20 is used to acquire the image of the focused device. The light emitted from the sample will pass through the lens to the monochromator and finally reaches the CCD camera (Figure 3-2-3 (b)). During the experiment, the box is covered by a piece of black cloth to reduce the interference from the light outside (Figure 3-2-3 (d)).

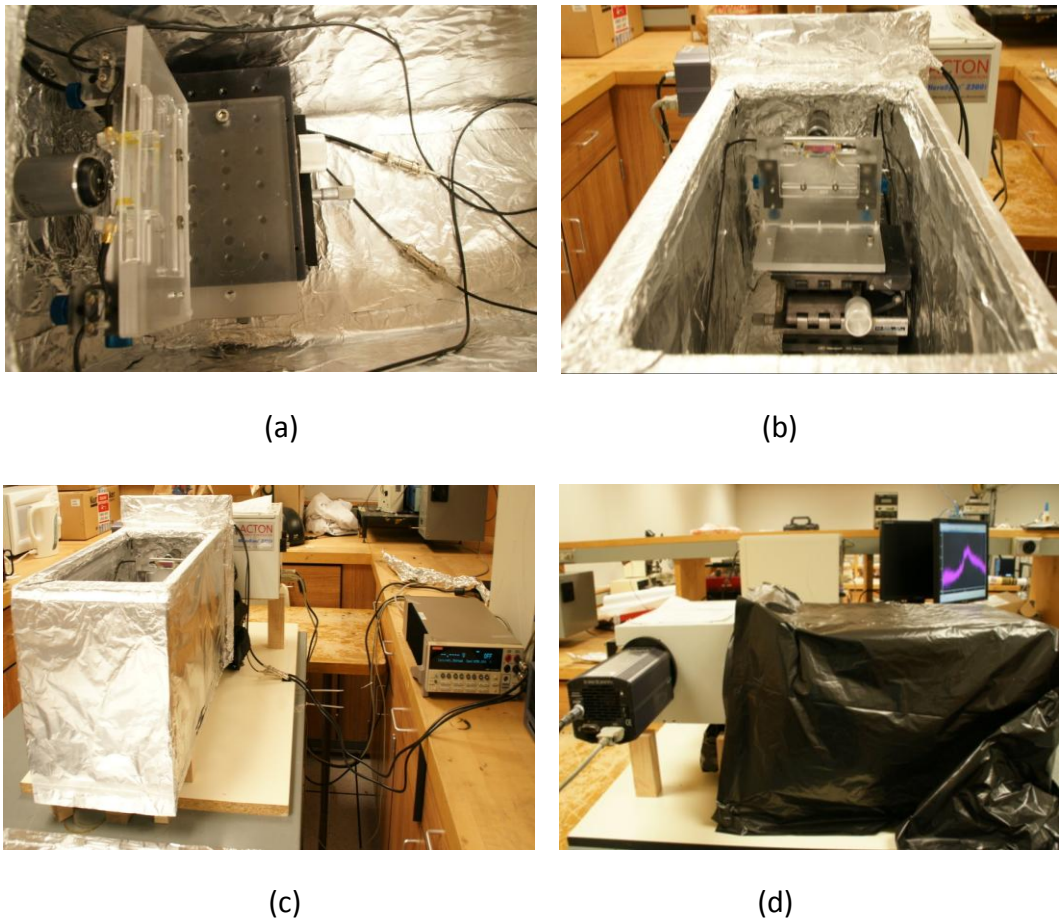

(a) (b)

(c) (d)

Figure 3-2-3. Experiment setup of the spectrum test: (a) device is fixed on the stage inside the box; (b) top view of the sample in the box; (c) device is connected to Keithley; (d) box is covered during the measurement.

The image that acquired by the CCD camera through the optical lens and the monochromator can be seen in the Winspec program in the computer. Figure 3-2-4 shows a focused S2 device with probes landing on it. The picture taken by the CCD camera has relatively low brightness. To make the image clear, the profile of the device and position of the probes are depicted.

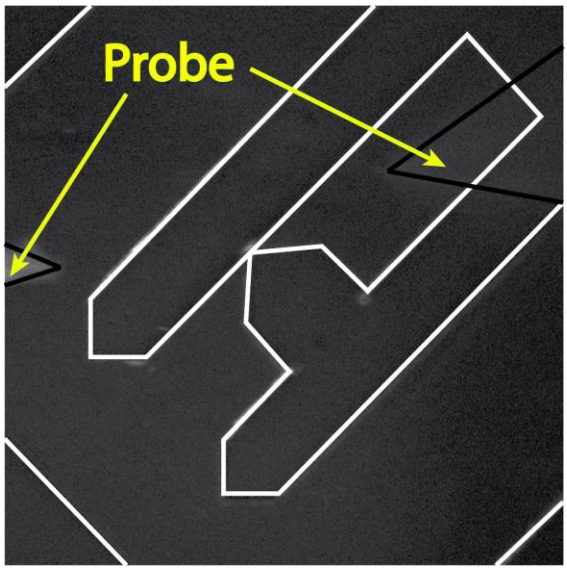

Figure 3-2-4. Image of the S2 device taken by CCD camera.

Figure 3-2-5 shows the electroluminescence from the position of the ZnO nanostructure of a S2 device when the whole box is covered with black cloth.

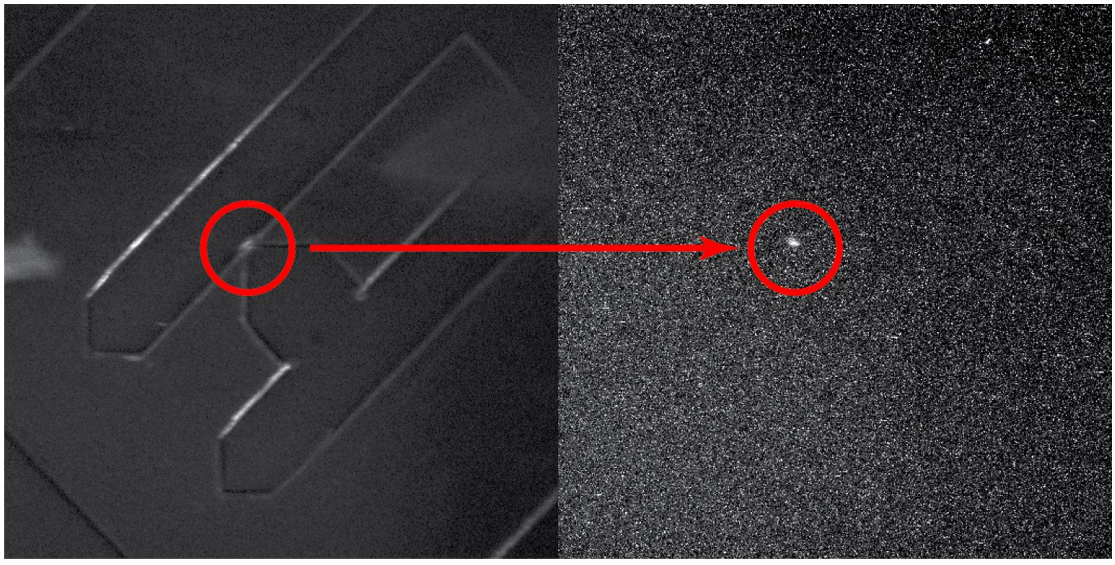

Figure 3-2-5. Image of the electroluminescence of the ZnO nanostructure taken by the CCD camera.

In the experiment, the light of wavelengths ranging from 200 nm to 1000 nm is set to be guided to the CCD camera. The test result is shown in Figure 3-2-6. It shows the spectrum of the light obtained from the nano-LED under four different current levels.

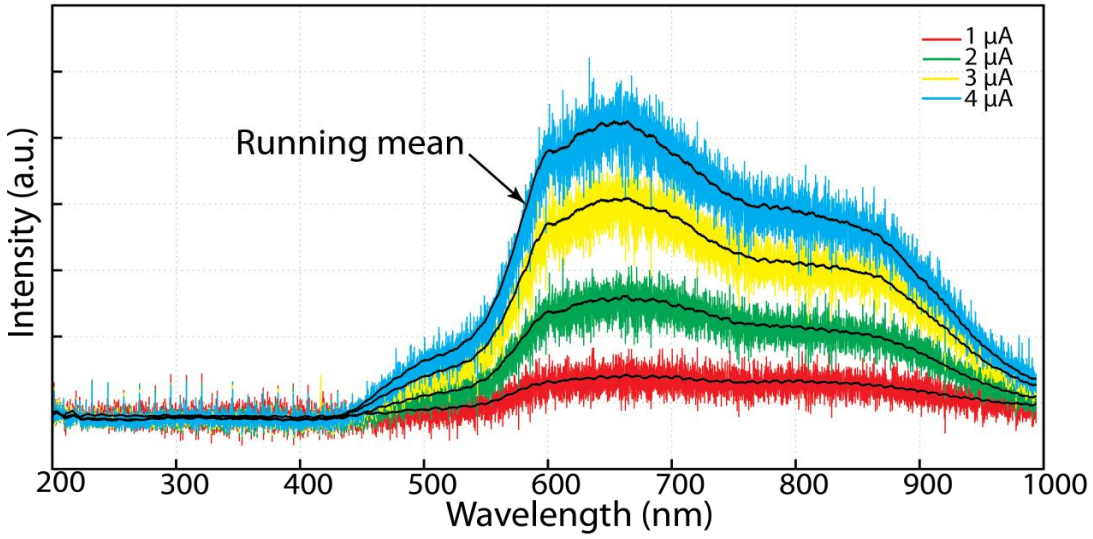

Figure 3-2-6. Spectrum of the light emitted from the device at different current levels.

The electroluminescence spectrum of the nano-LED is in the visible band ranging from 450nm to 1000nm. The major wavelengths are between 580nm and 850nm. When the current applied to the device increases, the intensity of the light increases, but the wavelengths are still the same. The visual spectrum is attributed to some intrinsic and extrinsic defects such as oxygen vacancies and Zn vacancies in ZnO. The mechanism of the visible wavelengths emitted from the device will be analyzed in the next chapter.

3.3 Intensity of the Light Emitted from Nano-LED at Different Voltage Levels

The intensity of the light emitted from the nano-LED is very low. Since the intensity of light is related to the number of photons, the nano-LED can be used to

generate small amount of photons or even single photon. With the number of photons that emitted from the device per second measured, if the frequency of the applied bias is high enough, it is possible for the nano-LED to emit only one single photon at a time. As the smallest unit of quantum computing, a single photon can store quantum information and it is potentially free from decoherence. Single photon emitters are essential components for realizing optical quantum computing[6].

With the same setup as in the spectrum test, the intensity of the emitted light with respect to different levels of applied voltage is measured. The voltage ranges from 10 to 40V. When the bias voltage is further increased, the ZnO nanostructure between the silicon tips may be broken by the high electric current that passes through it. At each measurement point, the light is integrated for several seconds. The values of the intensity obtained by the camera are then normalized to the intensity per second. The test result is shown in Figure 3-3-1.

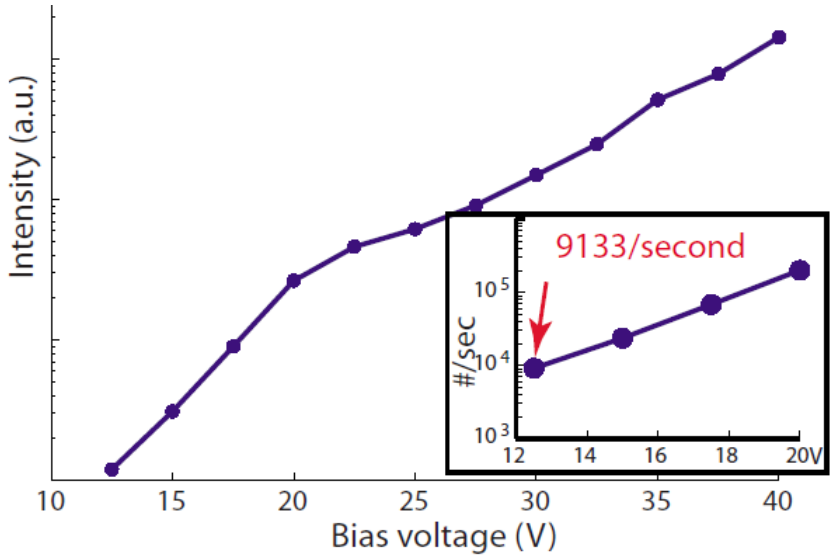

Figure 3-3-1. Measured intensity of the light emitted from the device at different voltages.

The turn-on voltage of the nano-LED for light emission is ~12 V. The intensity in the semi-log plot has two near linear slopes. It indicates that the light intensities are exponentially increasing. The break point voltage may result from the carrier injection saturation at one junction. The inset in Figure 3-3-1 shows the photon rate converted from the measured intensity. The photon rate at 12.5 V is estimated to be ~ 9000/s. When an ultra-short pulse near the turn on voltage is applied to the device, emission of one photon at a time could be possible.

3.4 I-V Curve Analysis of Nano-LED

In electronics, the current-voltage characteristic of a device is the relationship between the voltage across it and the current passes through it. The I-V characteristic of an electrical element can be used to determine a device's fundamental parameters and to analyze its behavior in electrical circuits. The shape of the I-V curve is determined by the transport of charge inside the device. For a diode, the current increases exponentially with forward bias while the current becomes negligible with reverse bias[73]. To explore the electronic structure of the nano-LED, the I-V curve of the device needs to be measured.

In a similar method as of the EL test, the I-V curve is measured by a HP4140B pA Meter/DC Voltage Source. The applied voltage from the source ranges from -25V to 25V with an increment of 1V and the value of the current is measured at each test point. The test result has been plotted in Figure 3-4-1.

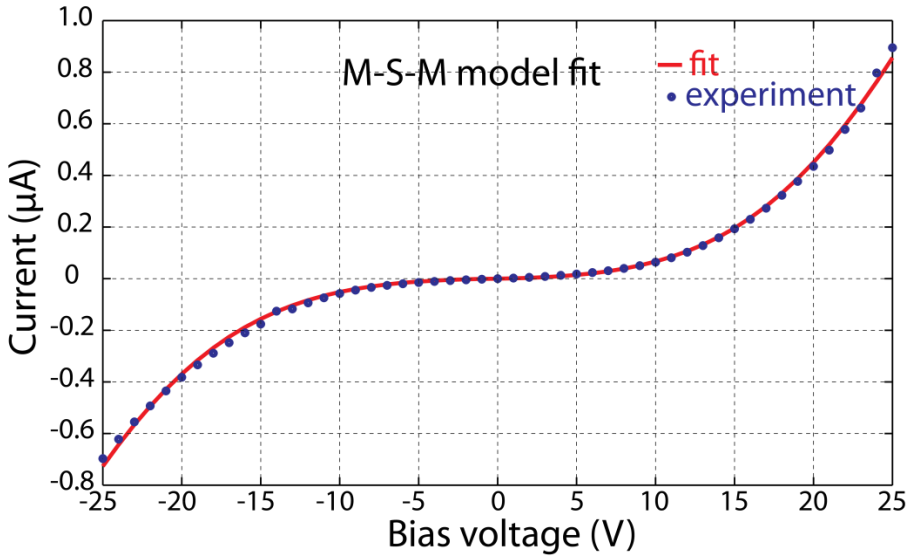

Figure 3-4-1. Measured I-V curve of the ZnO nanostructure between the nanogap.

The measured I-V data is fitted by the PKUMSM program[74]. As can be seen in Figure 3-4-1, the exponential curve shows typical characteristics of a diode structure. The semiconductor parameters of the device can be extracted from the fit. The values are listed in Table 3-4-1, where ϕ_1 and ϕ_2 are barrier heights of the junctions, R is the resistance of the nanostructure, N_d is the doping concentration, and μ_p is the carrier mobility.

Table 3-4-1. Extracted electrical parameters of ZnO nanostructure.

ϕ_1(eV)	ϕ_2(eV)	R(MΩ)	N_d(cm^{-3})	μ_p(cm^2/(V·s))
0.53	0.57	104	3.86×10^{17}	1.81×10^{-2}

The extracted barrier heights are asymmetrical and the values deviate from the calculated barrier heights, which may result from the formation of the Ni-Zn alloy during the thermal oxidation process to convert Zn to ZnO.

4 ANALYSIS OF ELECTRON TRANSPORT MECHANISMS IN METAL-SEMICONDUCTOR JUNCTIONS

For the nano-LED device, the emission of light can be explained by the electroluminescence mechanism from a metal-semiconductor-metal junction formed by Ni and ZnO. The electroluminescence requires injection of electrons and holes into the semiconductor. The source of the carrier transport in metal-semiconductor junctions needs to be investigated. In this chapter, the three main components of electron transport in Schottky diodes will be presented.

Electroluminescence is a light emission phenomenon caused by the electric current passing through a material. In semiconductors, electrons can be accelerated by a strong electric field. Electrons and holes will be excited and separated by the energetic electrons. When electrons and holes recombine in the material, the energy of the excited electrons will be released in the form of photons[45].

When Ni and ZnO are brought together, a Schottky barrier is formed. As can be seen in Figure 4-1, when a metal with work function $q\Phi_m$ is in contact with a semiconductor with work function $q\Phi_s$ ($\Phi_m > \Phi_s$), charge will transfer until the Fermi levels align at equilibrium. The electrostatic potential of the semiconductor is raised relative to that of the metal. A depletion region W is formed near the junction. In the depletion region, the positive charge due to uncompensated donor ions matches the negative charge on the metal. The equilibrium contact potential V_0 will prevent electron diffusion into the metal from the semiconductor. The potential barrier height Φ_B for electron injection into the semiconductor from the metal equals to $\Phi_m - \chi$, where $q\chi$ is the electron affinity. E_{Fm} and E_{Fs} are the Fermi level energy of the metal and the

semiconductor. E_C and E_V are the conduction band and valance band energy of the semiconductor[75].

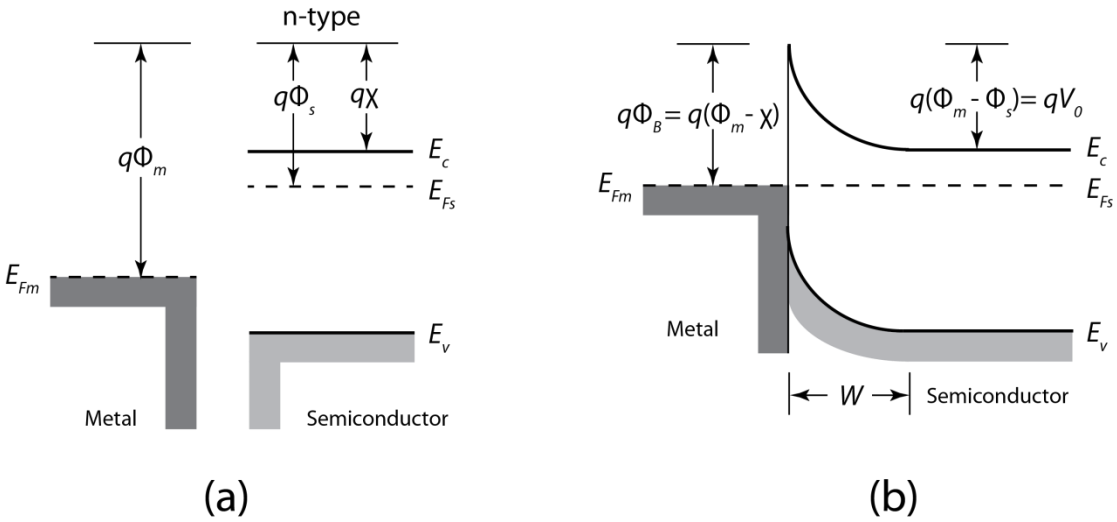

Figure 4-1. A Schottky barrier formed by contacting an n-type semiconductor with a metal (a) band diagrams of the metal and semiconductor before contacting; (b) band diagram for the junction at equilibrium.

When a Schottky barrier is under forward or reverse bias, the contact potential will change (Figure 4-2). When a forward-bias is applied to the Schottky barrier, the contact potential is reduced to $V_0 - V$ and V is the applied voltage. Electrons in the semiconductor conduction band can diffuse across the depletion region into the metal. Contrarily, the barrier height will increase by a reverse bias, which makes electron flow from semiconductor to metal negligible[75].

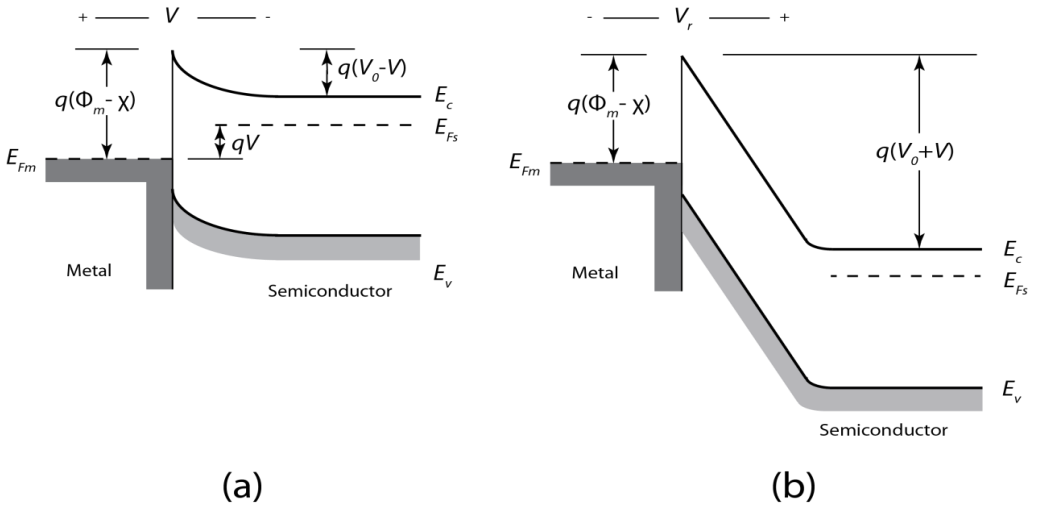

Figure 4-2. Forward and reverse bias on a Schottky barrier:
(a) forward bias; (b) reverse bias.

The transport of electrons in a Schottky diode consists of three components: thermionic emission, field emission and thermionic-field emission[76]. Figure 4-3 shows the qualitative current flow in a Schottky diode under bias.

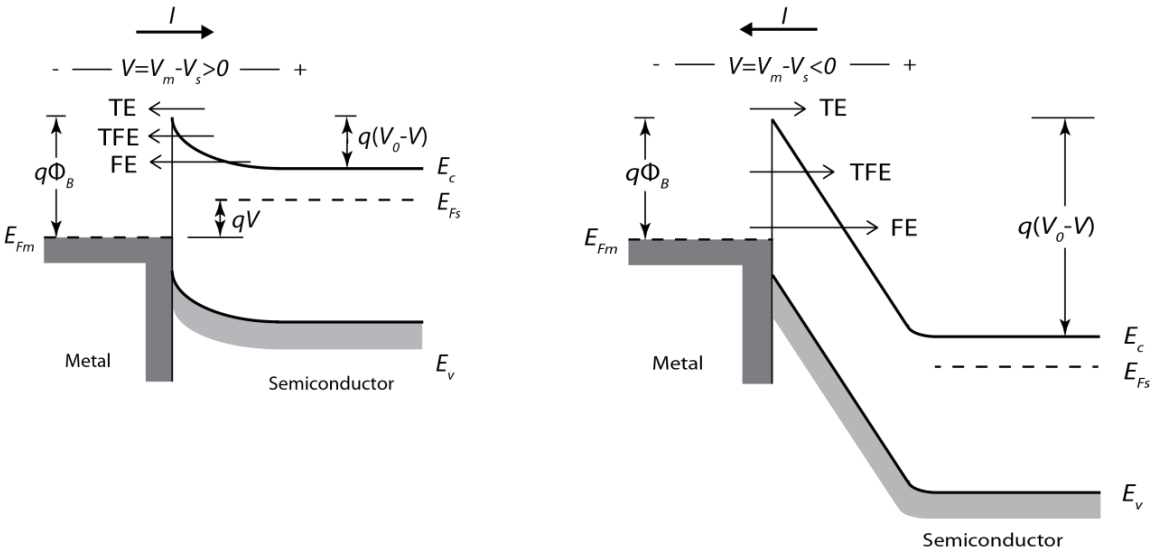

Figure 4-3. Energy-band diagram showing currents flow in a Schottky diode under bias: (a) forward bias; (b) reverse bias. TE = thermionic emission. FE = field emission. TFE = thermionic-field emission

Electrons transported by these three mechanisms together contribute to the current flow in the Schottky diode.

4.1 Thermionic Emission Theory

Thermionic emission is the charge carriers flow over a potential-energy barrier caused by the temperature. In ordinary condition, free electrons in the metal cannot leave the metallic surface. They are attracted by a strong force called surface barrier energy (E_B). When the temperature increases, some of the electrons inside the metal would obtain sufficient kinetic energy to overcome the surface barrier. The energy that needed for the emission of electrons to take place is the work function (W), that is

$$W = E_B - E_F \,. \tag{4.1}$$

In the equation, E_F is the Fermi level of energy of the metal. The relation between the number of electrons emitted by a unit area of the metallic surface and the temperature of the emitting materials is derived by Richardson and Dushman on the basis of Fermi-Dirac Statistics as in the equation below:

$$J = AT^2 e^{-W/kT} \,, \tag{4.2}$$

where J is the thermionic emission current density, $A = 4\pi mek^2 / h^3$ is the emission constant, T is the temperature, W is the work function of metal, k is the Boltzman constant, e is the electron charge, m is the electron mass, and h is the Plank's constant. The emission constant is the same for all the metals but the work function varies from metal to metal[77].

For a Schottky barrier formed in a metal-semiconductor junction, thermionic emission theory is applied as well. The theory assumes that the energetic carriers, which

have the energy larger than that at the interface of the junction, will cross the barrier and contribute to the current flow[76].

When a forward bias is applied to the Schottky barrier, the contact potential between the metal and the semiconductor is decreased. As can be seen in Figure 4-1-1, mobile electrons will flow from semiconductor to the metal, which result in the great increase in the cross barrier current. At the same time, a constant cross barrier electron flow from metal to semiconductor occurs since the potential barrier height (Φ_B) is not affected by the applied bias, but the resulting current is relatively small in the case of forward bias[76].

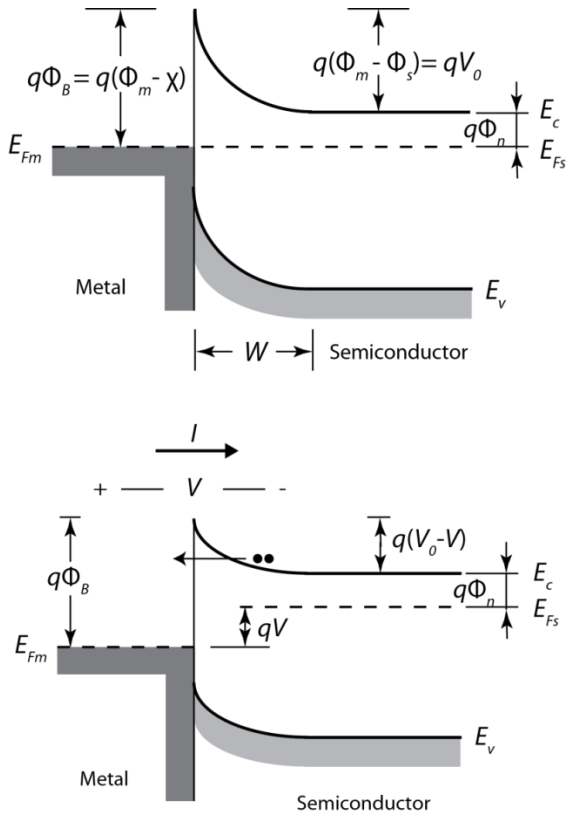

Figure 4-1-1. Thermionic emission in a Schottky barrier that is forward biased.

When the Schottky barrier is reverse biased, the cross barrier current attributed to electron flow from semiconductor to metal will decrease a lot, whereas the metal to semiconductor electron flow become visible as the saturation current[76]. Figure 4-1-2 shows the thermionic emission in a reverse biased Schottky barrier.

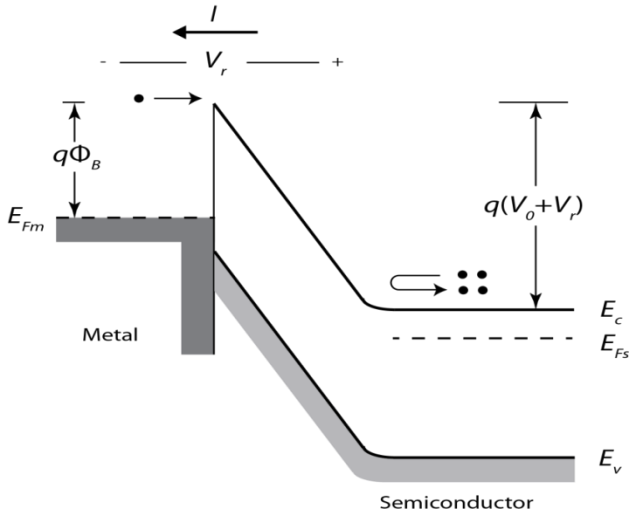

Figure 4-1-2. Thermionic emission in a Schottky barrier that is reverse biased.

The cross barrier current density from semiconductor to metal (J_{s-m}) is restricted by the concentration of electrons with kinetic energy (E) sufficient to surpass the barrier in the direction (x) of transport:

$$J_{s-m} = \int_{E_{Fm}+q\phi_B}^{\infty} qv_x dn\,, \tag{4.3}$$

where $E_{Fm}+q\phi_B$ is the minimum energy needed for electrons to inject into the metal because of thermionic emission, v_x is the carrier velocity in the direction of transport. The electron density between E and $E+dE$ is given by:

$$dn = N(E)F(E)dE\,, \tag{4.4}$$

where

$$N(E) = \frac{4\pi(2m^*)^{\frac{3}{2}}}{h^3}\sqrt{E - E_C} \tag{4.5}$$

is the density of states and m^* is the effective electron mass. And

$$F(E) = \frac{1}{e^{(E-E_{Fs})/kT}+1} \approx e^{-(E-E_{Fs})/kT} = e^{-[E-(E_c-q\phi_n)]/kT} = e^{-(E-E_c+q\phi_n)/kT} \tag{4.6}$$

is the Fermi-Dirac distribution function with $q\phi_n = E_C - E_{Fs}$. Assuming all the energy of electrons in the conduction band is kinetic energy, then:

$$E - E_C = \frac{1}{2}m^*v^2\,, \tag{4.7}$$

$$\sqrt{E - E_C} = v\sqrt{\frac{1}{2}m^*}\,, \tag{4.8}$$

$$dE = m^*v dv\,. \tag{4.9}$$

The electron density is given by:

$$\begin{aligned} dn &= N(E)F(E)dE \\ &= \frac{4\pi(2m^*)^{\frac{3}{2}}}{h^3}\sqrt{E - E_C}e^{-(E-E_c+q\phi_n)/kT}dE \\ &= \frac{4\pi(2m^*)^{\frac{3}{2}}}{h^3}\times v\sqrt{\frac{1}{2}m^*}\times e^{-q\phi_n/kT}\times e^{-\frac{m^*v^2}{2kT}}\times m^*v dv \\ &= 2\left(\frac{m^*}{h}\right)^3 e^{-q\phi_n/kT}e^{-\frac{m^*v^2}{2kT}}(4\pi v dv). \end{aligned}\,, \tag{4.10}$$

The above equation describes the number of electrons per unit volume that have velocities between v and $v+dv$ distributed over all directions. By resolving the velocity

into its components along the axes with the x-axis parallel to the transport direction, we have:

$$v^2 = {v_x}^2 + {v_y}^2 + {v_z}^2 , \tag{4.11}$$

$$4\pi v^2 dv = dv_x dv_y dv_z , \tag{4.12}$$

$$J_{s-m} = 2qe^{-q\phi_n/kT}\left(\frac{m^*}{h}\right)^3 \int_{v_{0x}}^{\infty} v_x e^{-\frac{m^* {v_x}^2}{2kT}} dv_x \int_{-\infty}^{\infty} e^{-\frac{m^* {v_y}^2}{2kT}} dv_y \int_{-\infty}^{\infty} e^{-\frac{m^* {v_z}^2}{2kT}} dv_z . \tag{4.13}$$

The velocity v_{0x} is the minimum velocity required in the x direction to surmount the barrier, which is given by:

$$\frac{1}{2} m^* {v_{0x}}^2 = q(V_0 - V) . \tag{4.14}$$

Using

$$\int_{-\infty}^{\infty} e^{-\frac{m^* {v_y}^2}{2kT}} dv_y = \int_{-\infty}^{\infty} e^{-\frac{m^* {v_z}^2}{2kT}} dv_z = \sqrt{\frac{2\pi kT}{m^*}} , \tag{4.15}$$

we have:

$$\begin{aligned} J_{s-m} &= 2qe^{-q\phi_n/kT}\left(\frac{m^*}{h}\right)^3 \int_{v_{0x}}^{\infty} v_x e^{-\frac{m^* {v_x}^2}{2kT}} dv_x \int_{-\infty}^{\infty} e^{-\frac{m^* {v_y}^2}{2kT}} dv_y \int_{-\infty}^{\infty} e^{-\frac{m^* {v_z}^2}{2kT}} dv_z \\ &= 2qe^{-q\phi_n/kT}\left(\frac{m^*}{h}\right)^3 \times \left(\frac{kT}{m^*} e^{-m{v_{0x}}^2/2kT}\right) \times \sqrt{\frac{2\pi kT}{m^*}} \times \sqrt{\frac{2\pi kT}{m^*}} \\ &= \frac{4\pi q m^* k^2}{h^3} T^2 e^{-q\phi_n/kT} e^{-q(V_0 - V)/kT} \\ &= A^* T^2 e^{-q(\phi_n + V_0)/kT} e^{qV/kT} \\ &= A^* T^2 e^{-q\phi_B/kT} e^{qV/kT} \end{aligned} , \tag{4.16}$$

and $A^* = \frac{4\pi q m^* k^2}{h^3}$ is the effective Richardson's constant. Since there is no net current flow at equilibrium, the cross barrier current density from semiconductor to metal (J_{m-s}) should be exactly opposite to the J_{s-m} when *V*=0, which is

$$J_{m-s} = -A^* T^2 e^{-q\phi_B/kT} . \tag{4.17}$$

Therefore, the total current density equation of the thermionic emission (J_n) for a metal-semiconductor junction is

$$J_n = J_{s-m} + J_{m-s} = A^* T^2 e^{-q\phi_B/kT} (e^{qV/kT} - 1) . \tag{4.18}$$

It can also be written as

$$J_n = J_{TE} (e^{qV/kT} - 1) , \tag{4.19}$$

where $J_{TE} = A^* T^2 e^{-q\phi_B/kT}$ is the barrier height dependent thermionic emission component[76]. In Equation 4.19, the exponential term describes the electron flux from semiconductor to metal and the -1 term describes the electron flux from metal to semiconductor.

4.2 Field Emission Theory

The field emission process is the emission of electrons induced by high electric field. Emission of electrons from solid or liquid surfaces into any non-conducting or weakly conducting dielectric and the promotion of electrons from valence band to conduction band in semiconductors can be regarded as field emission. The field emission is due to quantum mechanical effects, in which the potential barrier is narrowed by high electric field and electrons have the probability of tunneling through the barrier. Fowler-

Nordheim theory provides the quantitative description of this process. The current density J is given by the equation:

$$J = e\int_0^\infty n(E_x)D(E_x,F)dE_x\,, \tag{4.20}$$

where e is the electron charge, $n(E_x)$ is the number of electrons per second having energies between E_x and $E_x + dE_x$ on 1 cm^2 of the barrier surface from within the metal, F is the applied electric field, $E_x = p_x^2/2m$ is the electron kinetic energy carried by the momentum component p_x, m is the free electron rest mass, and $D(E_x,F)$ is the probability for the electron to tunnel through the potential barrier[78].

The tunneling may become significant for heavily doped semiconductors and for operation at low temperature. For a Schottky barrier, the tunneling current from semiconductor to metal ($J_{s-m(FE)}$) is proportional to the tunneling probability ($T(E)$) multiplied by the occupation probability in the semiconductor and the unoccupied probability in the metal. The following equation describes this current:

$$J_{s-m(FE)} = \frac{A^{**}T^2}{kT}\int_{E_{Fm}}^{E_{Fm}+q\phi_B} F_s T(E)(1-F_m)dE\,, \tag{4.21}$$

where F_m and F_s are the Fermi-Dirac distribution functions for the metal and the semiconductor. The tunneling probability depends on the width of the barrier at a particular energy. The tunneling current from metal to semiconductor ($J_{s-m(FE)}$) can also be written in similar form:

$$J_{m-s(FE)} = \frac{A^{**}T^2}{kT}\int_{E_C}^{E_{Fm}+q\phi_B} F_m T(E)(1-F_s)dE\,, \tag{4.22}$$

The sum of $J_{s-m(FE)}$ and $J_{s-m(FE)}$ is the net current density of field emission in a Schottky barrier[76]. Figure 4-2-1 shows field emission process in a Schottky barrier.

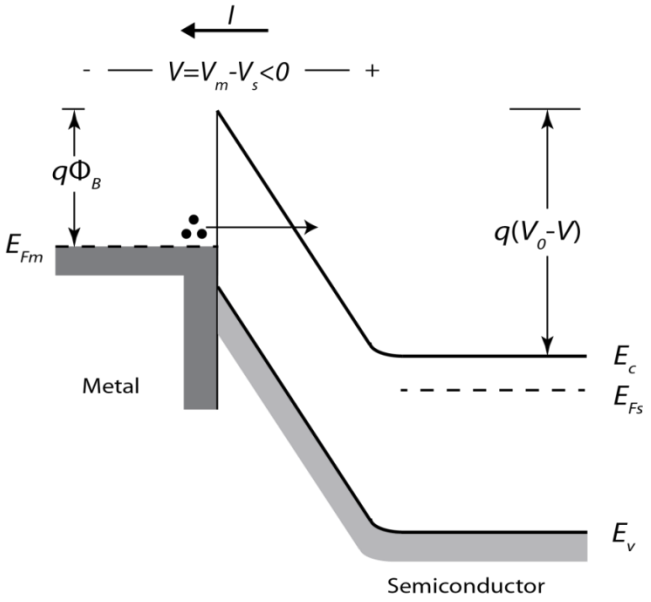

Figure 4-2-1. Field emission in a Schottky barrier that is reverse biased.

The current density $J_{s-m(FE)}$ induced by electrons tunneling from semiconductor to metal in the x-direction is

$$J = q\int_0^\infty v_x n(v_x) T(E_x) dv_x \,, \tag{4.23}$$

where $T(E_x)$ is the probability that one electron having energy E_x along the x-axis goes through the potential barrier. $n(v_x)dv_x$ is the density of electrons with velocity between v_x and $v_x + dv_x$ along the x-axis[78]. v_x, v_y and v_z are the components of the electron velocity (v), the total kinetic energy is

$$E_t = \frac{1}{2} m^* v^2 = E_x + E_y + E_z = \frac{1}{2} m^* (v_x{}^2 + v_y{}^2 + v_z{}^2) \,, \tag{4.24}$$

where E_x, E_y and E_z are the electron kinetic energy components along three axis. $n(v_x)$ can be obtained by the expression:

$$n(v_x) = \int_{-\infty}^{\infty} dv_y \int_{-\infty}^{\infty} dv_z F_s(\frac{1}{2}mv^2)[1-F_m(\frac{1}{2}mv^2)], \tag{4.25}$$

where F_s and F_m are the Fermi-Dirac distribution function, which are

$$F_s(\frac{1}{2}mv^2) = 2\frac{m^3}{h^3}\frac{1}{e^{(\frac{1}{2}mv^2-E_{Fs})/kT}+1}, \tag{4.26}$$

$$F_m(\frac{1}{2}mv^2) = 2\frac{m^3}{h^3}\frac{1}{e^{(\frac{1}{2}mv^2-E_{Fm})/kT}+1}. \tag{4.27}$$

The coordinates (v_y, v_z) can be considered in the polar coordinate (v_r, θ), which are $v_y = v_r\cos\theta$ and $v_z = v_r\sin\theta$. So we will have:

$$E_r = \frac{1}{2}m^*{v_r}^2 = E_y + E_z = \frac{1}{2}m^*({v_y}^2 + {v_z}^2), \tag{4.28}$$

and

$$dE_r = m^* v_r dv_r. \tag{4.29}$$

As $\int_{-\infty}^{\infty} dv_y \int_{-\infty}^{\infty} dv_z = \int_0^{2\pi} d\theta \int_0^{+\infty} v_r dv_r$, $n(v_x)$ becomes

$$\begin{aligned} n(v_x) &= \int_0^{2\pi} d\theta \int_0^{+\infty} v_r dv_r \int_{-\infty}^{\infty} F_s[\frac{1}{2}m^*({v_r}^2+{v_x}^2)]\{1-F_m[\frac{1}{2}m^*({v_r}^2+{v_x}^2)]\} \\ &= \frac{2\pi}{m^*}\int_0^{+\infty} dE_r F_s(E_r+E_x)[1-F_m(E_r+E_x)]. \end{aligned} \tag{4.30}$$

Considering $E_x = \frac{1}{2}m^*{v_x}^2$ and $dE_x = m^* v_x dv_x$, the current density then becomes

$$J = q\int_0^{\infty} v_x T(E_x)[\frac{2\pi}{m^*}\int_0^{+\infty} dE_r F_s(E_r + E_x)(1 - F_m(E_r + E_x))]dv_x$$
$$= \frac{2\pi q}{m^*}\int_0^{+\infty} dE_x T(E_x)\int_0^{+\infty} dE_r F_s(E_r + E_x)[1 - F_m(E_r + E_x)] \quad . \quad (4.31)$$
$$= \frac{2\pi q}{m^*}\int_0^{+\infty} dE_x T(E_x)\int_{E_x}^{+\infty} F_s(E)[1 - F_m(E)]dE$$

Considering the variable change $x = \frac{E - E_{Fs}}{kT}$, the second integral becomes

$$\int_{E_x}^{+\infty} F_s(E)[1 - F_m(E)]dE = \int_{E_x}^{+\infty} dE \frac{2m^3}{h^3}\frac{1}{e^{(\frac{1}{2}mv^2 - E_{Fs})/kT} + 1}[1 - \frac{2m^3}{h^3}\frac{1}{e^{(\frac{1}{2}mv^2 - E_{Fm})/kT} + 1}]$$
$$= \int_{\frac{E_x - E_{Fs}}{kT}}^{+\infty} dx \frac{2m^3}{h^3}\frac{1}{e^x + 1}[1 - \frac{2m^3}{h^3}\frac{1}{e^x e^{(E_{Fs} - E_{Fm})/kT} + 1}] \quad . (4.32)$$
$$= \{x*(\frac{2m^3}{h^3} - \frac{4m^6}{h^6}) - [\frac{2m^3}{h^3} + \frac{4m^6 \ln(e^x + 1)}{h^6(e^{(E_{Fs} - E_{Fm})/kT} - 1)} + \frac{4m^6 e^{(E_{Fs} - E_{Fm})/kT} \ln(e^x e^{(E_{Fs} - E_{Fm})/kT} + 1)}{h^6(e^{(E_{Fs} - E_{Fm})/kT} - 1)}\}\Big|_{\frac{E_x - E_{Fs}}{kT}}^{+\infty}$$

The tunneling probability $T(E_x)$ depends on the potential barrier shape and it can be calculated by the Wentzel-Kramers-Brillouin (WKB) approximation as

$$T(E_x) = \exp[-2\sqrt{\frac{8\pi^2 m^*}{h^2}}\int_0^{Ttun} \sqrt{q\phi(x) - E_x}dx], \quad (4.33)$$

where $q\phi(x) - E_x$ is the difference between the energy of the potential barrier at the position x and the electron energy in the x-direction. The first two terms of Taylor's series expansion of the function $g(E_x) = \sqrt{q\phi(x) - E_x}$ around the Fermi level of the metal can be expressed as

$$g(E_x) = g(E_{Fm}) + \frac{dg(E_x)}{dE_x}\Big|_{E_x = E_f} \cdot (E_x - E_{Fm})$$
$$= \sqrt{q\phi(x) - E_{Fm}} - \frac{1}{2\sqrt{q\phi(x) - E_{Fm}}}(E_x - E_{Fm}) \quad . \quad (4.34)$$

The tunneling probability becomes

$$T(E_x) = \exp[-2\sqrt{\frac{8\pi^2 m^*}{h^2}}\int_0^{Ttun}[\sqrt{q\phi(x)-E_{Fm}} - \frac{1}{2\sqrt{q\phi(x)-E_{Fm}}}(E_x - E_{Fm})]dx$$

$$= \exp[-2\sqrt{\frac{8\pi^2 m^*}{h^2}}\int_0^{Ttun}(\sqrt{q\phi(x)-E_{Fm}}dx) + \sqrt{\frac{8\pi^2 m^*}{h^2}}\int_0^{Ttun}\frac{1}{\sqrt{q\phi(x)-E_{Fm}}}(E_x - E_{Fm})dx]. \quad (4.35)$$

$$= T(E_{Fm})\exp[\sqrt{\frac{8\pi^2 m^*}{h^2}}\int_0^{Ttun}\frac{1}{\sqrt{q\phi(x)-E_{Fm}}}(E_x - E_{Fm})dx]$$

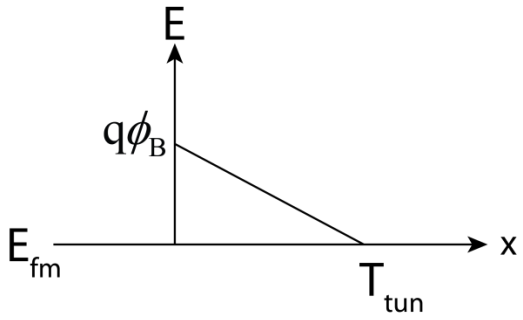

Figure 4-2-2. Electrical potential of the barrier.

Assuming that the barrier shape is triangular (Figure 4-2-2), the resultant potential for the triangular barrier at a distance x away from the origin can be expressed as

$$q\phi(x) = q\phi_B + E_{Fm} - q\varepsilon x, \quad (4.36)$$

where $q\phi(x)$ is the energy at point x and ε is the effective electric field. We also have $q\phi_B - q\varepsilon Ttun = 0$, so $T(E_{Fm})$ can be calculated as

$$
\begin{aligned}
T(E_{Fm}) &= \exp[-2\sqrt{\frac{8\pi^2 m^*}{h^2}}\int_0^{Ttun}(\sqrt{q\phi(x)-E_{Fm}}dx)] \\
&= \exp[-2\sqrt{\frac{8\pi^2 m^*}{h^2}}\int_0^{Ttun}(\sqrt{q\phi_B - q\varepsilon x}dx] \\
&= \exp\{-2\sqrt{\frac{8\pi^2 m^*}{h^2}}\cdot[\frac{2}{3q\varepsilon}(q\phi_B - q\varepsilon x)^{\frac{3}{2}}]\Big|_0^{Ttun}\} \qquad . \qquad (4.37) \\
&= \exp[-2\sqrt{\frac{8\pi^2 m^*}{h^2}}\cdot\frac{2}{3q\varepsilon}(q\phi_B)^{\frac{3}{2}}] \\
&= \exp[-\frac{4}{3}\sqrt{\frac{8\pi^2 m^* q}{h^2}}\frac{(\phi_B)^{\frac{3}{2}}}{\varepsilon}].
\end{aligned}
$$

The current density then becomes

$$
\begin{aligned}
J &= \frac{2\pi q}{m^*}\int_0^{+\infty} dE_x T(E_x)\int_{E_x}^{+\infty} F_s(E)F_m(E)dE \\
&= \frac{2\pi q}{m^*}\int_0^{+\infty}\{dE_x \exp[-\frac{4}{3}\sqrt{\frac{8\pi^2 m^* q}{h^2}}\frac{(\phi_B)^{\frac{3}{2}}}{\varepsilon}]\cdot\exp[\sqrt{\frac{8\pi^2 m^*}{h^2}}\int_0^{Ttun}\frac{1}{\sqrt{q\phi(x)-E_{Fm}}}(E_x - E_{Fm})dx]\} \qquad . \qquad (4.38) \\
&= \{x^*(\frac{2m^3}{h^3}-\frac{4m^6}{h^6})-[\frac{2m^3}{h^3}+\frac{4m^6\ln(e^x+1)}{h^6(e^{(E_{Fs}-E_{Fm})/kT}-1)}+\frac{4m^6 e^{(E_{Fs}-E_{Fm})/kT}\ln(e^x e^{(E_{Fs}-E_{Fm})/kT}+1)}{h^6(e^{(E_{Fs}-E_{Fm})/kT}-1)}\}\Big|_{\frac{E_x-E_{Fs}}{kT}}^{+\infty}
\end{aligned}
$$

Further calculation of the above equation would be complex.

A widely used analytical approximation of the field emission was proposed by Padovani and Sratton in 1966[80]. A rough criterion to evaluate the relative contributions of the components of thermionic emission, field emission and thermionic-field emission can be set by comparing the thermal energy kT with the energy E_{00}, which is defined as

$$
E_{00} \equiv \frac{q\hbar}{2}\sqrt{\frac{N}{m^*\varepsilon_s}}, \qquad (4.39)
$$

where ε_s is the dielectric constant of the semiconductor and N is the doping concentration of the semiconductor[76]. When $kT >> E_{00}$, thermionic emission is the

dominant mechanism. When $kT << E_{00}$, field emission dominates. When $kT \approx E_{00}$, the main mechanism is thermionic filed emission. Under forward bias, the field emission current can be expressed as

$$J_{FE} = \frac{A^{**}T\pi \exp[-q(\phi_B - V_F)/E_{00}]}{c_1 k \sin(\pi c_1 kT)}[1-\exp(c_1 q V_F)], \tag{4.40}$$

where $c_1 \equiv \frac{1}{2E_{00}}\log[\frac{4(\phi_B - V_F)}{\phi_n}]$. Under reverse bias, the field emission current can be expressed as

$$J_{FE} = A^{**}(\frac{E_{00}}{k})^2\left(\frac{\phi_B + V_R}{\phi_B}\right)\exp(-\frac{2q(\phi_B)^{\frac{2}{3}}}{3E_{00}\sqrt{\phi_B + V_R}}). \tag{4.41}$$

The above equation can be used to estimate the field emission current in a Schottky barrier.

4.3 Thermionic-Field Emission Theory

Thermionic-field emission of electrons takes place when a high electric field is applied on a solid body under relatively high temperature. Compared with the sum of the thermionic emission and field emission current densities, the current density of the thermionic-field emission could be several orders of magnitude larger than it. While field emission usually happens near the Fermi level, thermionic-field emission happens at the energy between thermionic emission and field emission. The thermally excited carriers see a thinner barrier than field emission[81].

Figure 4-3-1 shows the thermionic-field emission of electrons in a reverse biased Schottky barrier.

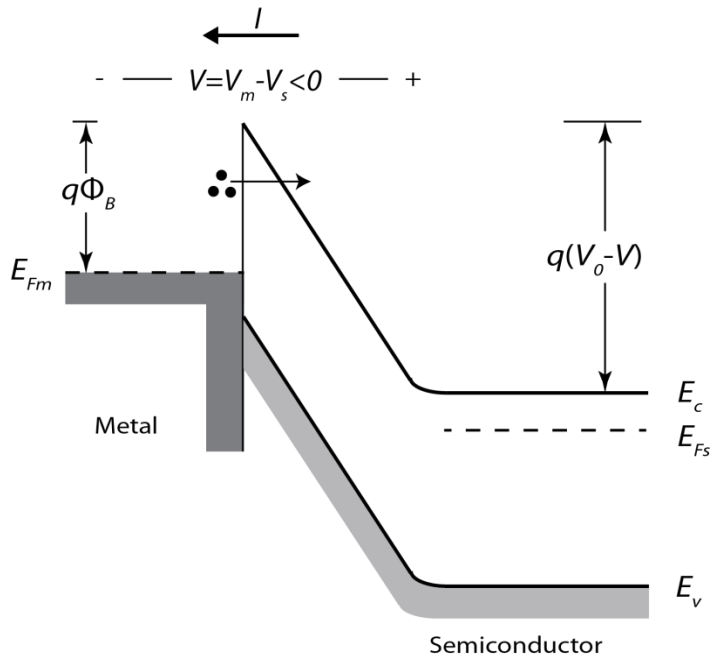

Figure 4-3-1. Thermionic-field emission in a Schottky barrier that is reverse biased.

Under forward bias, thermionic-field emission current can be expressed as

$$J_{TFE} = \frac{A^{**}T\sqrt{\pi E_{00} q(\phi_B - \phi_n - V_F)}}{k\cosh(E_{00}/kT)} \exp[\frac{-q\phi_n}{kT} - \frac{q(\phi_B - \phi_n)}{E_0}] \exp(\frac{qV_F}{E_0}), \qquad (4.42)$$

where $E_0 = E_{00}\coth(\frac{E_{00}}{kT})$. Under reverse bias, the current is given by:

$$J_{TFE} = \frac{A^{**}T}{k}\sqrt{\pi E_{00} q[V_R + \frac{\phi_B}{\cosh^2(E_{00}/kT)}]} \exp(\frac{-q\phi_B}{E_0}) \exp(\frac{qV_R}{\varepsilon'}), \qquad (4.43)$$

where $\varepsilon' = \frac{E_{00}}{(E_{00}/kT) - \tanh(E_{00}/kT)}$. The above equations are proposed by Padovani and Sratton[80]. They can be used to calculate the current of thermionic-field emission in a Schottky barrier.

In our nano-LED devices, it is believed that the three mechanisms presented above together contribute to the electron transport. However, since the dielectric constant of the oxidized ZnO and its temperature are unknown, the dominant mechanism of these three cannot be determined.

5 DISCUSSIONS

Based on the analysis in the previous chapter, the light-emitting mechanisms of the nano-LED device and the source of the EL spectrum are going to be investigated in this section. When the bias is applied to the Ni-ZnO-Ni junction, electrons and holes are injected into the ZnO nanostructure. Photons are emitted from the nanostructure when the electrons and holes combine. The EL spectrum is believed to result from some intrinsic defects.

5.1 Metal-Semiconductor-Metal Junction

For the nano-LED, the Ni on the suspended silicon tips and the ZnO nanostructure between the nanogap form a metal-semiconductor-metal (MSM) junction.

A typical MSM junction can be seen in Figure 5-1-1.

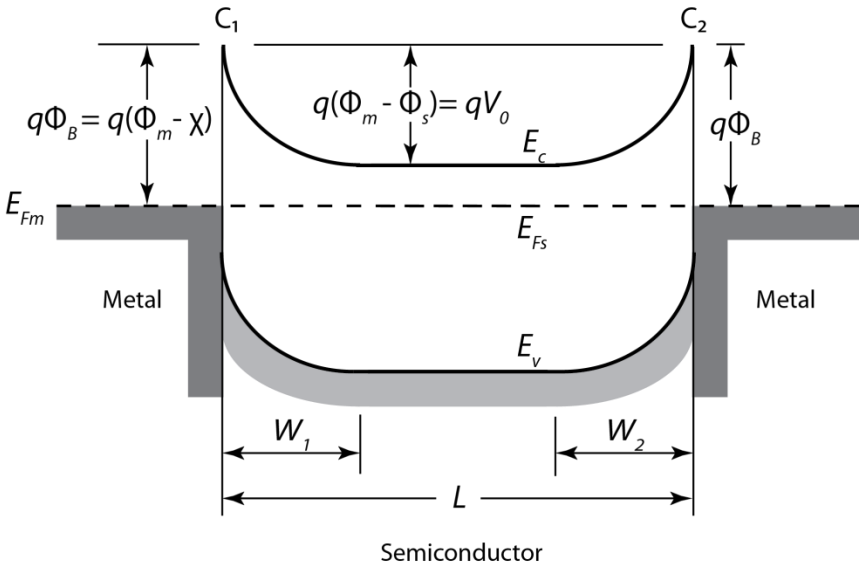

Figure 5-1-1. Schematic diagram of a metal-semiconductor-metal junction.

Basically, the MSM junction has the structure of two Schottky barriers connected back to back. When a voltage is applied, one of the contacts is reverse biased and the other is forward biased. As the voltage increases, the depletion widths of the junctions (W_1 and W_2) will also increase until the sum of the depletion widths equals to the length of the semiconductor (L) in the middle. The voltage at this point is called reach-through voltage. Figure 5-1-2 shows the potential profile of the MSM structure under a bias with negative side on the left. The left contact (C_1) is reverse biased and the right contact (C_2) is forward biased[82].

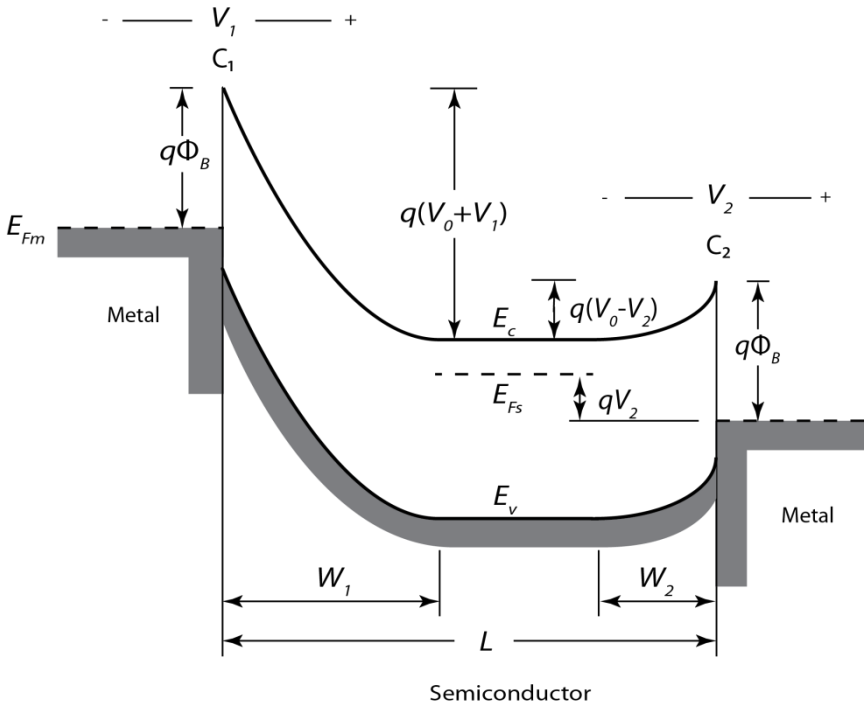

Figure 5-1-2. Potential profile of the MSM structure under bias with positive bias on contact 2.

The two contacts share the applied voltage V, with

$$V = V_1 + V_2 \tag{5.1}$$

As derived before, the current density of C_1 due to thermionic emission is

$$J_{n1} = A^* T^2 e^{-q\Phi_B/kT}(1 - e^{-qV_1/kT}). \tag{5.2}$$

The current density of C_2 due to thermionic emission is

$$J_{n2} = A^* T^2 e^{-q\Phi_B/kT}(e^{-qV_2/kT} - 1). \tag{5.3}$$

For current continuity, we will have:

$$J_{n1} = J_{n2}. \tag{5.4}$$

By solving Equation 5.1 and Equation 5.4, the current density can be acquired.

Before the reach-through voltage, thermionic emission of electrons from C_1 is the main cause of the current flow. With further increase in the applied voltage, the current results from the injection of holes at the forward-bias contact increases rapidly because of the lowering of hole barrier. Thermionic emission of the holes from metal to the semiconductor constitutes the hole current (Figure 5-1-3).

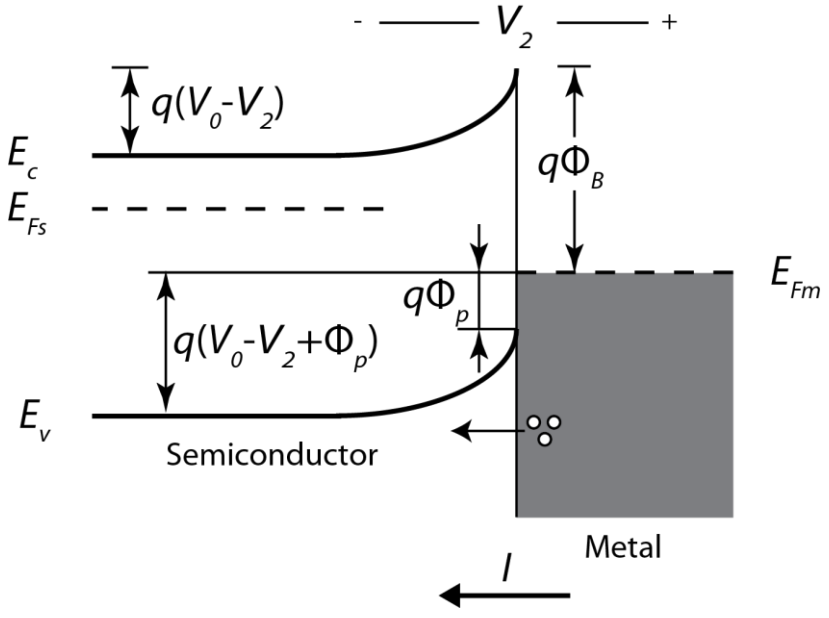

Figure 5-1-3. Hole injection at the forward-biased metal-semiconductor junction.

The current density of the hole current at the forward-biased junction can be described by the following equation:

$$J_{p2} = A_p^* T^2 e^{-q(\Phi_B + V_0 - V_2)/kT}. \quad (5.5)$$

In the case of the Ni-ZnO-Ni junction, the work function of Ni ($q\Phi_m$) is reported to be 5.15 eV. ZnO has the work function ($q\Phi_s$) of 4.45 eV and the electron affinity ($q\chi$) of 4.29 eV[83, 84]. At equilibrium, the depletion width of the Ni-ZnO junction can be calculated in the following equation[75]:

$$W = \sqrt{\frac{2\varepsilon_s \varepsilon_0 V_0}{qN_d}}, \quad (5.6)$$

where $qV_0 = q\Phi_m - q\Phi_s = 5.15\text{eV} - 4.45\text{eV} = 0.7\text{eV}$, $V_0 = \frac{0.7\text{eV}}{q} = 0.7\text{V}$,

$q = 1.6\times10^{-19}\text{C}$, $\varepsilon_0 = 8.85\times10^{-14}\text{F/cm}$ is the permittivity of free space, $\varepsilon_s = 7.8$ is the relative dielectric constant of ZnO, and $N_d = 10^{17}\text{cm}^{-3}$ is the doping concentration of ZnO. So, the depletion width of a Ni-ZnO Schottky diode is calculated to be

$$W = \sqrt{\frac{2\varepsilon_s \varepsilon_0 V_0}{qN_d}} = \sqrt{\frac{2\times7.8\times8.85\times10^{-14}\times0.7}{1.6\times10^{-19}\times10^{17}}} = 77.7\text{nm}.$$

Since the average size of the nanogaps is less than 100 nm. The Ni-ZnO-Ni junction is fully depleted at equilibrium (Figure 5-1-4).

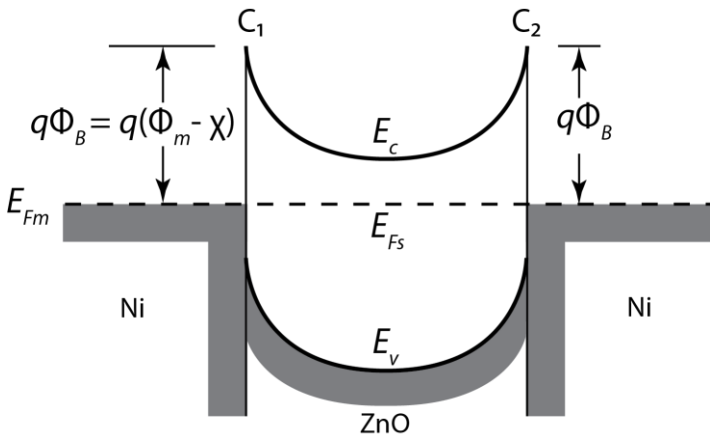

Figure 5-1-4. Schematic diagram of the Ni-ZnO-Ni junction at equilibrium.

Figure 5-1-5 shows the energy band diagram of the Ni-ZnO-Ni junction under bias. The electroluminescence mechanism is explained in Figure 5-1-6.

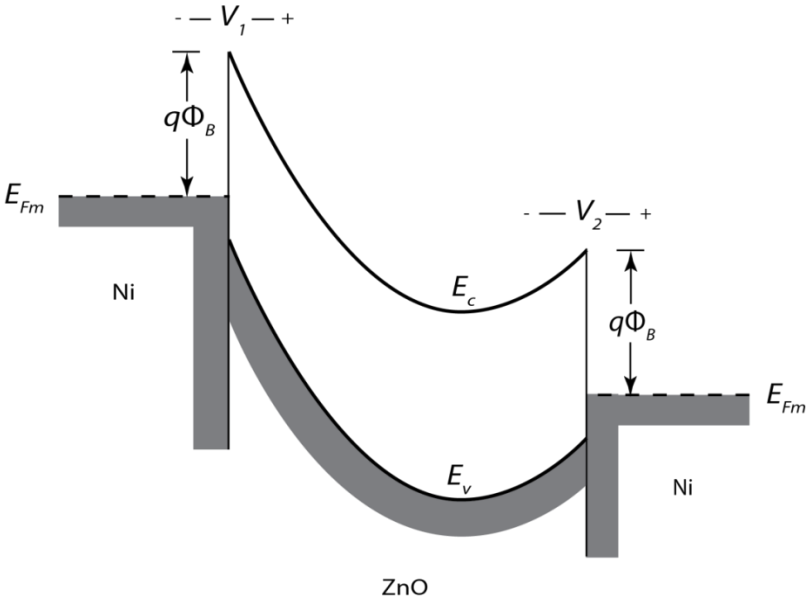

Figure 5-1-5. Schematic diagram of the Ni-ZnO-Ni junction under bias with positive on the right side.

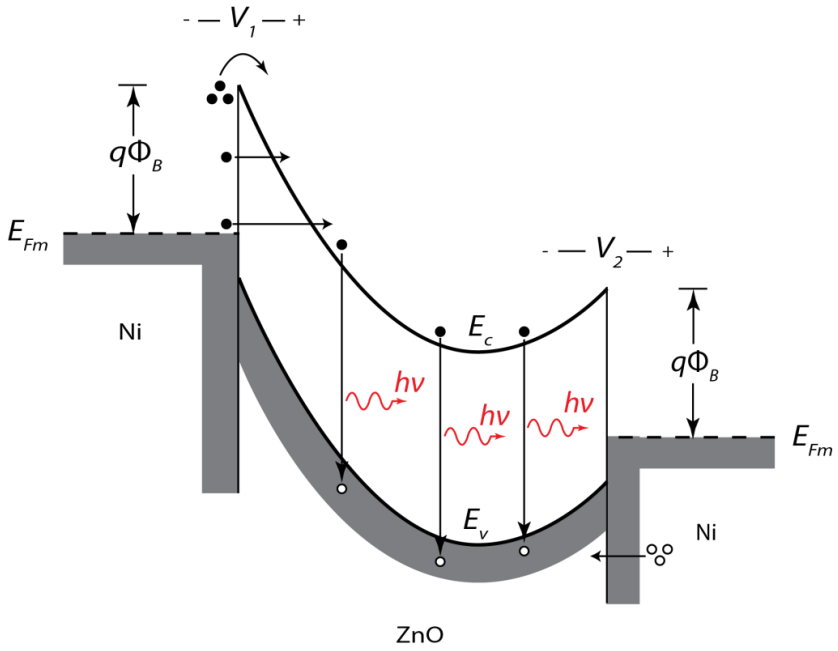

Figure 5-1-6. Schematic diagram of the electroluminescence of Ni-ZnO-Ni junction under bias.

At the left contact which is reverse-biased, thermionic emission, thermionic-field emission and field emission result in the electron current. At the right contact which is forward-biased, holes are injected from Ni to ZnO due to thermionic emission. When the injected electrons and holes combine in ZnO, photons are emitted.

5.2 Source of ZnO Spectrum

As mentioned earlier, ZnO exhibits dissimilar spectra in different conditions. Generally, ultraviolet (UV) near-band-edge emission and defect-related deep level emissions are observed from ZnO. The behavior and the position of the deep level emissions strongly depend on the growth methods of ZnO, the measurement techniques

of the spectrum, and specific parameters taken in each experiment by different researchers[64-71].

The photoluminescence spectra of ZnO are usually found to contain both near UV emission and deep level emissions[64-68, 85].

Wang et al. have measured the PL spectra from thermal oxidized Zn films deposited by filtered cathodic vacuum arc technique. They have observed UV emission peak at around 3.3 eV and a green band emission around 2.4 eV when the oxidation temperature is under 750 ℃ and a yellow emission band around 2.1 eV when the oxidation temperature is higher than 800 ℃. The yellow luminescence is thought to be induced by intrinsic defects formed at high temperature[64].

Baca et al. have got the UV transition and a strong green band around 2.4 eV from ZnO films formed by thermal oxidation of polycrystalline Zn foils[65].

The PL spectra obtained by Hsieh et al from ZnO films deposited on SiO2/Si substrates by radio frequency (RF) magnetron sputtering have showed both UVemission and green emission that is located at 523 nm[66]. By comparing the spectra of the ZnO annealed at different conditions, they have concluded that the emission of green light results from oxygen vacancies.

The PL studies of ZnO films made by oxidation of Zn films deposited on fused silica substrates by direct current magnetron sputtering are conducted by Cho et al[67]. They have observed a single peak around 390 nm that is corresponding to ZnO free exciton emission for wavelengths between 370 nm and 675 nm. The defects related deep level emission is negligible in their research.

Ahn et al. have investigated the PL spectra of ZnO layers grown by various methods[85]. For the ZnO film grown by RF magnetron sputtering, the visible emission consists of orange-red, green, and violet wavelengths. Oxygen interstitial (O_i), oxygen vacancy (V_o) and Zn interstitial (Zn_i) are responsible for these emissions respectively. For the samples grown by MOCVD, blue and green emissions are observed at a low oxygen rate while blue and orange-red emissions are observed in oxygen rich conditions. The blue emission is thought to be related to Zn vacancy (V_{Zn}) and the green and orange-red emissions are corresponding to V_o and O_i respectively. The PL spectra of ZnO nanorods grown by MOCVD exhibit intense UV emission. The PL spectra of ZnO nanorods grown by thermal oxidation show an intense green emission that is associated with $V_{o.}$

The defect emissions from different ZnO nanostructures have been conducted by Djurisic et al using photoluminescence measurement method. The ZnO needles show orange-red defect emission, the ZnO shells show green defect emission and the ZnO rods exhibit yellow defect emission[68]. Possible explanation for the phenomena is that green and yellow emissions result from the excitation below the band edge while the orange-red emission comes from excitation above the band edge.

The studies of cathodoluminescence spectra of ZnO are also conducted by many researchers[69-71].

The CL spectra of ZnO tested by Ohashi et al. consist of green emission at 2.2 eV and yellow emission at 2.0 eV[69]. They have claimed that donor-acceptor pair emissions involving V_{Zn} and lighium (Li) acceptors are attributed to the green and yellow emission respectively.

Radoi et al. have reported the CL spectra of mechanical milled ZnO samples[70]. Near band edge UV emission including shallow levels and dislocation related emission and green-yellow band deep level emission have been observed.

Bano et al. have fabricated Au/ZnO Schottky light-emitting diodes by low temperature aqueous chemical methods[71]. EL and CL measurements have been conducted to study the optical properties of ZnO. Near band edge emission and a strong deep level emission centered at 690 nm exhibit in the CL spectra. The deep level emission is related to the defect concentration at the interface and self-absorbed UV emission.

The EL spectrum from Bano's research shows two deep level emission peaks. The green peak located at 533 nm is considered to result from oxygen vacancies and the read peak centered at 700 nm is related to zinc vacancies[71].

Although a lot of experiments and theoretic works have been done to find the origin of the visible spectrum from ZnO, no consensus has been reached[85-91]. More research needs to be conducted to solve this problem.

In crystals, there are three basic classes of defects[92]. Point defects refer to the missing atoms or the atoms in irregular space in the lattice. Lattice vacancies, self-interstitials, substitutional impurities, and interstitial impurities belong to point defects. Line defects, also known as dislocations, are groups of atoms in irregular positions. Two ideal types are edge dislocation and screw dislocation. In a material, grain boundaries, stacking faults and external surfaces are called planar defects.

Point defects are the most common defects. When atoms change their positions frequently and randomly, empty lattice sites are left behind, which are known as

vacancies. When the temperature is high, the number of vacancies will be larger because atoms will jump between equilibrium positions more frequently. The number of vacancies increases exponentially with the absolute temperature and it can be described by the following equation:

$$N_V = N_S \exp(-E_V / kT), \tag{5.7}$$

where N_V is the number of vacancies, N_S is the number of regular lattice sites, and E_V is the energy required for a vacant lattice site. Interstitials refer to the atoms stay between regular lattice sites. Self-interstitial happens when the interstitial atoms and the lattice atoms are the same. Smaller foreign atoms such as carbon, nitrogen, hydrogen or oxygen atoms are called interstitial impurities. When a matrix atom is replaces by a foreign atom, the impurity is called a substitutional impurity.

The spectrum of nanostructured ZnO is strongly affected by surface defects because of the large surface-to volume ratio. ZnO has a relatively open structure. Therefore ZnO has many sites to accommodate defects[91]. Zn interstitials are shown to be shallow donors. Zn interstitials are not stable at room temperature because they are fast diffusers with low migration barrier. It is shown that the oxygen vacancy is a deep donor. The level of the O vacancy is calculated to be 0.5-0.8 eV above the maximum value of the valence band. Other calculations estimate it to be 1-2 eV below the conduction band minimum. Zn vacancies are double acceptors. Calculations find the acceptor levels of Zn vacancies to be 0.1-0.2 eV and 0.9-1.2 eV above the valence band maximum. Oxygen interstitials are deep acceptors. The transition levels are derived to be 0.72 and 1.59 eV above the valence band maximum. Figure 5-2-1 shows some of the defect levels within the bandgap of ZnO[85-92].

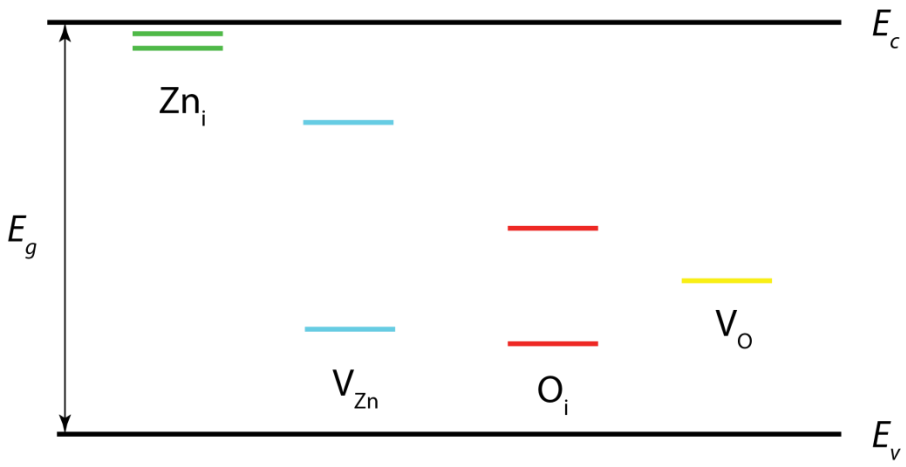

Figure 5-2-1. Energy levels of native defects in ZnO.

In our research, the EL spectrum exhibits a broad visual band with major peaks between 580 nm and 850 nm. It is believed that the visual spectrum is attributed to some intrinsic and extrinsic defects such as oxygen vacancies and zinc vacancies. There is no near band edge UV emission observed, which maybe because the carrier density in EL is lower compared to that in PL. In this condition, the recombination of the carriers at defect levels surpasses the recombination of the carriers from the band edge in ZnO.

6 CONCLUSION

In conclusion, nano-LED devices have been fabricated and investigated. Nanogap devices have been fabricated on SOI wafers by optical lithography and two-step KOH wet chemical silicon etching. ZnO nanostructures have been synthesized between the nanogaps after evaporation of Ni and Zn and the oxidation of Zn. Metal-semiconductor-metal junctions are formed by Ni and ZnO. Electroluminescence has been observed when bias is applied to the device. I-V curve, EL spectrum and EL light intensity of the devices have been measured. The structure of the metal-semiconductor-metal junction is depicted as two back to back connected Schottky diodes. The electroluminescence mechanism has been analyzed. When electrons from thermionic emission, field emission and thermionic-field emission from metal to semiconductor at the reverse-biased junction combine with the holes injected to the semiconductor from the metal at the forward-biased junction, photons are emitted from ZnO nanostructure. The EL spectrum shows broad visual band wavelengths. The visual band wavelengths are believed to result from intrinsic defects of ZnO such as oxygen vacancies and zinc vacancies. The nano-LED devices have many potential applications as light sources in electronics and biomedicine. It is also shown that the devices have the possibility to work as single photon emitters for quantum computing.

7 FUTURE WORK

More theoretical and experimental work need to be done in the future to optimize the devices.

Detailed formation of the wavelengths of the spectrum needs to be explored. By comparing the spectrum of the devices that oxidized at different temperature for different periods of time, various colors of the wavelengths could be related to specific intrinsic defects. Devices of adjustable light wavelengths may be realized by controlling the parameters of the fabrication process.

The dominant electron transport mechanism in MSM junctions needs to be investigated. According to the theories of thermionic emission, field emission and thermionic-field emission, electron transport in Schottky diodes depends on potential barrier height, temperature, doping concentration of ZnO, dielectric constant of ZnO, and the voltage applied to the junction. With one of the parameters mentioned above varied and others fixed, the current density of the three mechanisms may be quantified and the dominant mechanism can be determined.

More research needs to be conducted to increase the quality of the devices, such as the stability, reliability, repeatability. For example, the efficiency of the light-emission from the device may be improved by choosing better material as the electrical contact for ZnO.

REFERENCES

[1] Kimberly Patch and Eric Smalley. (2004, February). "Nanomechanics and nanoelectronics: Molecule-size machines." *Technology Research News*. [On-line] Available: http://www.trnmag.com/mtfnanomechanics.html [June 1, 2012].

[2] Tsutomu Araki and Hiroaki Misawa. "Light emitting diode-based nanosecond ultraviolet light source for fluorescence lifetime measurements." *Review of Scientific Instruments*, vol. 66, no. 12, pp. 5469-5472, 1995.

[3] Gordon T Kennedy, Daniel S Elson, Jonathan D Hares, Ian Munro, Vincent Poher, Paul M W French, and Mark A A Neil. "Fluorescence lifetime imaging using light emitting diodes." *J. Phys. D: Appl. Phys.*, vol. 41, no. 9, 094012, May 2008.

[4] H Xu, J Zhang, K M Davitt, Y-K Song, and A V Nurmikko. "Application of blue–green and ultraviolet micro-LEDs to biological imaging and detection." *J. Phys. D: Appl. Phys.*, vol. 41, no. 9, 094013, May 2008.

[5] Valéry Zwiller, Thomas Aichele, and Oliver Benson. "Quantum optics with single quantum dot devices." *New Journal of Physics*, vol. 6, 96, 2004.

[6] Jeremy L. O'Brien. "Optical Quantum Computing." *Science*, vol. 318, no. 5856, pp. 1567-1570, 2007.

[7] Christelle Monat, Blandine Alloing, Carl Zinoni, Lianhe H. Li, and Andrea Fiore. "Nanostructured Current-Confined Single Quantum Dot Light-Emitting Diode at 1300 nm." *Nano letters*, vol.6, no.7 pp.1464-1467, 2006.

[8] Linus C. Chuang, Forrest G. Sedgwick, Roger Chen, Wai Son Ko, Michael Moewe, Kar Wei Ng Thai-Truong D. Tran, and Connie Chang-Hasnain. "GaAs-Based Nanoneedle Light Emitting Diode and Avalanche Photodiode Monolithically Integrated on a Silicon Substrate." *Nano Letters*, vol 11, no. 2, pp. 385-390, 2011.

[9] Athavan Nadarajah, Robert C. Word, Jan Meiss, and Rolf Ko1nenkamp. "Flexible Inorganic Nanowire Light-Emitting Diode." *Nano Letters*, vol. 8, no. 2, pp. 534-537, 2008.

[10] Substrate Chih-Han Chen, Shoou-Jinn Chang, Sheng-Po Chang, Meng-Ju Li, I-Cherng Chen,|Ting-Jen Hsueh, An-Di Hsu, and Cheng-Liang Hsu. "Fabrication of a White-Light-Emitting Diode by Doping Gallium into ZnO Nanowire on a p-GaN Substrate." *J. Phys. Chem. C*, vol. 114, no.29, pp. 12422–12426, 2010.

[11] Zhanao Tan, Fan Zhang, Ting Zhu, and Jian Xu. "Bright and Color-Saturated Emission from Blue Light-Emitting Diodes Based on Solution-Processed Colloidal Nanocrystal Quantum Dots." *Nano Letters*, vol. 7, no. 12, pp. 3803-3807, 2007.

[12] Jeonghun Kwak, Wan Ki Bae, Donggu Lee, Insun Park, Jaehoon Lim, Myeongjin Park, Hyunduck Cho, Heeje Woo, Do Y. Yoon, Kookheon Char, Seonghoon Lee, and Changhee Lee. "Bright and Efficient Full-Color Colloidal Quantum Dot Light-Emitting Diodes Using an Inverted Device Structure." *Nano Letters*, 2012, 12, 2362−2366

[13] Wei Guo, Meng Zhang, Animesh Banerjee, and Pallab Bhattacharya. "Catalyst-Free InGaN/GaN Nanowire Light Emitting Diodes Grown on (001) Silicon by Molecular Beam Epitaxy." *Nano Letters*, vol. 10, pp. 3355–3359, 2010.

[14] R. Ko1nenkamp, R. C. Word, and M. Godinez. "Ultraviolet Electroluminescence from ZnO/Polymer Heterojunction Light-Emitting Diodes." *Nano Letters*, vol. 5 no.10, pp. 2005-2008, 2005.

[15] Jiming Bao, Mariano A. Zimmler, Federico Capasso, Xiaowei Wang and Z. F. Ren. "Broadband ZnO Single-Nanowire Light-Emitting Diode." *Nano Letters*, vol. 6, no. 8, pp.1719-1722, 2006.

[16] Ya-Ping Hsieh, Hsin-Yi Chen, Ming-Zhang Lin, Shu-Chia Shiu, Mario Hofmann, Ming-Yau Chern, Xiaoting Jia, Ying-Jay Yang, Hsiu-Ju Chang, Hsuan-Ming Huang, Shao-Chin Tseng, Li-Chyong Chen, Kuei-Hsien Chen, Ching-Fuh Lin, X Chi-Te Liang, and Yang-Fang Chen. "Electroluminescence from ZnO/Si-Nanotips Light-Emitting Diodes." *Nano Letters*, vol. 9, no. 5, pp. 1839-1843, 2009.

[17] H. Elgala, R. Mesleh, H. Haas and B. Pricope. "OFDM Visible Light Wireless Communication Based on White LEDs," in *Proceedings of the 64th IEEE Vehicular Technology Conference*, 2007, pp. 2185-2189.

[18] T. Komine and M. Nakagawa. "Integrated system of white LED visible-light communication and power-line communication," in *IEEE Transactions on Consumer Electronics*, 2003, vol. 49 , no. 1, pp. 71 – 79.

[19] J. Ramsden. "What is nanotechnology?" *Nanotechnology perceptions*, vol. 1 no. 1, pp. 3-17, 2005.

[20] Fritz Allhoff, Patrick Lin, and Daniel Moore. *What is nanotechnology and why does it matter: from science to ethics*. Malden, MA: Wiley-Blackwell, 2010, pp. 3-12.

[21] Karl Goser, Peter Glösekötter, and Jan Dienstuhl. *Nanoelectronics and nanosystems: from transistors to molecular and quantum devices*. Berlin, NY: Springer, 2004, pp. 1-4.

[22] Carmen M. Lilley and Qiaojian Huang. "Electrical Properties of Metallic Nanowires for Nanoelectronic Applications" in *Nanoelectronics: nanowires, molecular electronics, and nanodevices* 1st ed. Krzysztof Iniewski, Ed. New York: McGraw-Hill, 2011, pp.3-5.

[23] Chun-yen Chang. "The highlights in the Nano world." in *Proceedings of the IEEE*, 2003, vol. 91, no. pp1756-1764.

[24] Kinneret Keren, Rotem S. Berman, Evgeny Buchstab, Uri Sivan, and Erez Braun. "DNA-Templated Carbon Nanotube Field-Effect Transistor." *Science* 21 November 2003: Vol. 302 no. 5649 pp. 1380-1382, 2003.

[25] Claes Thelander, Martin H. Magnusson, Knut Deppert, Lars Samuelson, Per Rugaard Poulsen, Jesper Nygård, and Jørn Borggreen. "Gold nanoparticle single-electron transistor with carbon nanotube leads." *Appl. Phys. Lett.*, vol. 79, pp. 2106, 2001.

[26] Adrian Bachtold, Peter Hadley, Takeshi Nakanishi and Cees Dekker. "Logic Circuits with Carbon Nanotube Transistors." S*cience*, vol. 294, no. 5545, pp. 1317-1320, 2001.

[27] J. B. Cui, R. Sordan, M. Burghard, and K. Kern. "Carbon nanotube memory devices of high charge storage stability." *Appl. Phys. Lett.*, vol. 81, pp. 3260, 2002.

[28] J. Song, W. Dongmok, M. C. McAlpine, R. S. Friedman, W. Yue, and C. M.Lieber, "Scalable interconnection and integration of nanowire devices without registration." *Nano Letters*, vol. 4, pp. 915-919, 2004.

[29] A. Husain, J. Hone, H. W. C. Postma, X. M. H. Huang, T. Drake, M. Barbic, A. Scherer, and M. L. Roukes, "Nanowire-based very-high-frequency electromechanical resonator." *Applied Physics Letters*, vol. 83, pp. 1240-1242, 2003.

[30] R. Moradian and A. Fathalian, "Ferromagnetic semiconductor single-wall carbon nanotubes." *Nanotechnology*, vol. 17, pp. 1835-1842, 2006.

[31] Mark S. Gudiksen , Lincoln J. Lauhon, Jianfang Wang, David C. Smith and Charles M. Lieber. "Growth of nanowire superlattice structures for nanoscale photonics and electronics." *Nature*, 415, pp. 617-620, 2002.

[32] Lincoln J. Lauhon, Mark S. Gudiksen , Deli Wang, and Charles M. Lieber. "Epitaxial core–shell and core–multishell nanowire heterostructures." *Nature*, vol. 420, pp. 57-61, 2002.

[33] Zhaohui Zhong, Deli Wang, Yi Cui, Marc W. Bockrath, and Charles M. Lieber. "Nanowire Crossbar Arrays as Address Decoders for Integrated Nanosystems." *Science*, vol. 302, no. 5649, pp. 1377-1379, 2003.

[34] Guido Burkard. "Electron Spins in Quantum Dots as Qubits for Quantum Information Processing Guido Burkard and Daniel Loss," in *Semiconductor*

Spintronics and Quantum Computations, 1st ed. D. D. Awshalom, D. Loss, and N. Samarth, Ed. Berlin, Germany: Springer-Verlag, 2002, pp. 229-276.

[35] Michael Wilson, Kamali Kannangara, Geoff Smith, Michelle Simmons, and Burkhard Raguse. *Nanotechnology basic science and emerging technologies*. Boca Raton, FL: Chapman & Hall/CRC, 2002, pp. 168-170.

[36] Ottilia Saxl. "Opportunities for industry in the application of nanotechnology." Internet: http://www.nano.org.uk/members/FreeReports/applications.pdf. [May 30, 2012].

[37] Young Han Choe and Venkatesen Mauree. "The optical world: ITU-T technology watch report." Internet: http://www.itu.int/ITU-T/newslog/The+Optical+World.aspx, June 2011 [June 1, 2012].

[38] M Arumugam. "Optical fiber communication - An overview." *Pramana - journal of physics*, vol. 57, pp. 849–869, 2001.

[39] N. N. Ledentsov, "Quantum dot VCSELs," in *Digest of the LEOS Summer Topical Meetings*, 1999, pp. I15–I16.

[40] J. Phillips, P. Bhattacharya, S. W. Kennerly, D. W. Beekman, and M. Dutta, "Self-assembled InAs-GaAs quantum-dot intersubband detectors," in *IEEE J. Quantum Electronics*, vol. 35, pp. 936–943, 1999.

[41] Yun Xing and Jianghong Rao. "Quantum dot bioconjugates for *in vitro* diagnostics & *in vivo* imaging." *Cancer Biomarkers*, vol. 4, pp. 307-319, 2008.

[42] E. Knill, R. Laflamme, and G. J. Milburn. "A scheme for efficient quantum computation with linear optics." *Nature*, vol. 409, pp. 46-52, 2001.

[43] Ineke Malsch. "Biomedical Applications of Nanotechnology." *The Industrial Physicist*, vol. 8, no. 3, pp. 15-17, 2002.

[44] S. M. Sze and Kwok K. Ng. "LEDs and Lasers." in *Physics of Semiconductor Devices*, 3rd Edition. S. M. Sze and Kwok K. Ng, Ed. Hoboken, New Jersy: John Wiley & Sons, Inc., 2007, pp. 601-657.

[45] Ben G. Streetman and Sanjay Kumar Banerjee. "Excess carriers in semiconductors." in *Solid state electronic devices*, 6th ed. Ben G. Streetman and Sanjay Kumar Banerjee, Ed. Upper Saddle River, NJ: Pearson Prentice Hall, 2006, pp.118-130.

[46] E. Fred Schubert. "LED basics: Electrical properties." in *Light-emitting diodes*, 2nd edition. E. Fred Schubert, Ed. Cambridge, UK: New York: Cambridge University Press, 2006, pp. 59-83.

[47] Leah Bergman and Jeanne L. McHale. *Handbook of luminescent semiconductor materials*. Boca Raton, FL: CRC Press, 2012, pp.21-252.

[48] C. W. Tang and S. A. VanSlyke. "Organic electroluminescent diodes." *Appl. Phys. Lett*., vol. 51, no. 12, pp. 913-915, 1987.

[49] Jayesh Bharathan and Yang Yang. "Polymer electroluminescent devices processed by inkjet printing: I. Polymer light-emitting logo." *Appl. Phys. Lett.*, vol. 72, no. 21, pp. 2660 -2662, 1998.

[50] M. A. Baldo, D. F. O'Brien, Y. You, A. Shoustikov, S. Sibley, M. E. Thompson, and S. R. Forrest. "Highly efficient phosphorescent emission from organic electroluminescent devices." *Nature*, vol.395, pp. 151-154, 1998.

[51] E. Fred Schubert. "Communication LEDs." in *Light-emitting diodes*, 2nd edition. E. Fred Schubert, Ed. Cambridge, UK: New York: Cambridge University Press, 2006, pp. 382-391.

[52] Zhiliang Yuan, Beata E. Kardynal, R. Mark Stevenson, Andrew J. Shields , Charlene J. Lobo, Ken Cooper, Neil S. Beattie, David A. Ritchie and Michael Pepper. "Electrically Driven Single-Photon Source." *Science,* vol. 295 no. 5552, pp. 102-105, 2002.

[53] W J O'Hagan, M McKenna, D C Sherrington, O J Rolinski, and D J S Birch. "MHz LED source for nanosecond fluorescence sensing*." Measurement Science and Technology*, vol. 13, no. 1, pp.84, 2002.

[54] P. Herman, B.P. Maliwal, H.–J. Lin, and J.R.Lakowicz. "Frequency-domain fluorescence microscopy with the LED as a light source." *Journal of Microscopy*, vol. 203, pp. 176-181, 2001.

[55] H. Morkoc. "GaN and Silicon Carbide as Optoelectronic Materials," in *The Handbook of Photonics*, 1st ed. Mool Chand Gupta, Ed. CRC Press, 1997, pp. 49-81.

[56] Bill Moats. "Gallium Arsenide vs. Silicon." Internet: http://www2.ensc.sfu.ca/~jones/ENSC100/Gamma/gallium.html, Dec. 1, 1996 [June 1, 2012].

[57] Anderson Janotti and Chris G Van de Walle. "Fundamentals of zinc oxide as a semiconductor." *Rep. Prog. Phys.*, vol. 72, 126501, 2009.

[58] "Markets for zinc oxide in electronics." Internet: http://nanomarkets.net/market_reports/report/markets_for_zinc_oxide_in_electronics#, March 2009 [June 2, 2012].

[59] Ü. Özgür, Ya. I. Alivov, C. Liu, A. Teke, M. A. Reshchikov, S. Doğan, V. Avrutin, S.-J. Cho, and H. Morkoç "A comprehensive review of ZnO materials and devices." *J. Appl. Phys,* vol. **98**, 041301, 2005.

[60] Pu Xian Gao and Zhong L. Wang. "Nanoarchitectures of semiconducting and piezoelectric zinc oxide." *Journal of Applied Physics*, vol. 97, 044304, 2005.

[61] An-Jen Cheng. "One dimensional zinc oxide nanostructures for optoelectronic applications: solar cells and photodiodes." Doctor dissertation, Auburn University, USA, 2008.

[62] S.J. Peartona, D.P. Nortona, K. Ipa, Y.W. Heoa, T. Steinerb. "Recent progress in processing and properties of ZnO." *Superlattices and Microstructures*, vol. 34, pp. 3–32, 2003.

[63] Ashok K. Sood, Zhong Lin Wang, Dennis L. Polla, Nibir K. Dhar, Tariq Manzur4 and A.F.M. Anwar. "ZnO Nanostructures for Optoelectronic Applications," in *Optoelectronic Devices and Propertie*s, Oleg Sergiyenko, Ed. InTech, April 2011, pp. 173-195.

[64] Y.G. Wang a, S.P. Lau, X.H. Zhang, H.W. Lee, S.F. Yu B.K. Tay, H.H. Hng. "Evolution of visible luminescence in ZnO by thermal oxidation of zinc films." *Chemical Physics Letters,* vol.375, pp.113–118, 2005.

[65] R Baca, G Juárez, H Solache, J Andraca, J Martinez, O Garcia, T Kryshtab and R Peña-Sierra. "Kinetics of the oxidation of Zn foils in air atmosphere." *Materials Science and Engineering*, vol. 8, pp. 012043, 2010.

[66] P.-T. Hsieh, Y.-C. Chen, K.-S. Kao, and C.-M. Wang. "Luminescence mechanism of ZnO thin film investigated by XPS measurement." Appl. Phys. A, vol. 90, pp. 317-321, 2008.

[67] Sunglae Cho, Jing Ma, Yunki Kim, Yi Sun, George K. L. Wong, and John B. Kettersonb. "Photoluminescence and ultraviolet lasing of polycrystalline ZnO thin films prepared by the oxidation of the metallic Zn." *Applied Physics Letters*, vol. 75, issue no. 18, 1999.

[68] A. B. Djurišić, Y. H. Leung, K. H. Tam, L. Ding, W. K. Ge, H. Y. Chen, and S. Gwo. "Green, yellow, and orange defect emission from ZnO nanostructures: Influence of excitation wavelength." *Applied Physics Letters*, vol.88, 103107, 2006.

[69] Naoki Ohashi, Naoki Ebisawa, Takashi Sekiguchi, Isao Sakaguchi, Yoshiki Wada, Tadashi Takenaka, and Hajime Haneda. "Yellowish-white luminescence in codoped zinc oxide." *Applied Physics Letters*, vol. 86, 091902, 2005.

[70] R Radoi, P Fernández, J Piqueras, M S Wiggins and J Solis. "Luminescence properties of mechanically milled and laser irradiated ZnO." *Nanotechnology*, vol. 14, no. 7, pp. 794-798, 2003.

[71] Bano, N., Hussain, I., Nur, O., Willander, M., Kwack, H. S., Le Si Dang, D. "Study of Au/ZnO nanorods Schottky light-emitting diodes grown by low-temperature aqueous chemical method." *Applied Physics A*, vol. 100, issue 2, pp.467-472.

[72] J. H. Han, N. Yoshimizu, T. Cheng, M. Ziwisky, S. A. Bhave, A. Lal, and C.-H. Lee. "Nano-Electromechanical Zero-Dimensional Freestanding Nanogap Actuator", Proc. MEMS, 2011, pp. 1357-1360.

[73] Donald A Neamen. *Microelectronics: circuit analysis and design*. New York: McGraw-Hill, 2007, pp. 26-32.

[74] Z. Zhang, K. Yao, Y. Liu, C. Jin, X. Liang, Q. Chen, and L.-M. Peng. "Quantitative analysis of current-voltage characteristics of semiconducting nanowires: decoupling of contact effects." *Advanced functional materials*, vol. 17, no. 14, pp. 2478-2489, 2007.

[75] Ben G. Streetman and Sanjay Kumar Banerjee. "Junctions." in *Solid state electronic devices*, 6th ed. Ben G. Streetman and Sanjay Kumar Banerjee, Ed. Upper Saddle River, NJ: Pearson Prentice Hall, 2006, pp.227-234.

[76] S. M. Sze and Kwok K. Ng. "Metal-Semiconductor Contact." in *Physics of Semiconductor Devices*, 3rd Edition. S. M. Sze and Kwok K. Ng, Ed. Hoboken, New Jersy: John Wiley & Sons, Inc., 2007, pp. 601-657.

[77] Uma Mukherji. *Engineering physics*. Oxford, U.K.: Alpha Science, 2007, pp. 57-68.

[78] George Fursey. *Field emission in vacuum microelectronics*. New York: Kluwer Academic/Plenum Publishers, 2005, pp. 1-6.

[79] Doris Ng Keh Ting. "Synthesis and characterization of gallium nitride nanowires by pulsed laser ablation." Doctor dissertation, National University of Singapore, Singapore, 2008.

[80] F.A. Padovani, R. Stratton. "Field and thermionic-field emission in Schottky barriers." *Solid-State Electronics*, vol. 9, issue 7, Pages 695–707, 1966.

[81] Sylvain Coulombe and Jean-Luc Meunier. "Thermo-field emission: a comparative study." J. Phys. D: Appl. Phys., vol. 30, pp. 776-780, 1997.

[82] S. M. Sze, D. J. Coleman, JR. and A. Loya. "Current transport in metal-semiconductor-metal (MSM) structures." *Solid-State Electronics*, vol. 14. pp. 1209-1218, 1971.

[83] Min-Ho Kim, Sung-Nam Lee, Chul Huh Serng Yerl Park, Jeong Yeul Han, Jae Myung Seo, and Seong-Ju Park. "Interfacial reaction and Fermi level movement induced by sequentially deposited metals on GaN: Au/Ni/GaN." *Physics Review B,* vol. 61, no. 16, pp. 10966- 10971, 2000.

[84] Sanghyun Ju. "A study of nanowire transistors and their applications for flexible and transparent electronics." Doctor dissertation, Purdue University, IN, 2007.

[85] Cheol Hyoun Ahn, Young Yi Kim, Dong Chan Kim, Sanjay Kumar Mohanta, and Hyung Koun Choa. "A comparative analysis of deep level emission in ZnO layers deposited by various methods." *Journal Of Applied Physics,* vol. 105, pp. 013502, 2009.

[86] Zhao Lei, Lian Jian-she, Liu Yu-hua, Jiang Qing. "Influence of preparation methods on photoluminescence properties of ZnO films on quartz glass." *Transactions of Nonferrous Metals Society of China,* vol. 18, issue 1, pp. 145–149, 2008.

[87] Nidhal. N. Jandowa, Kamarul Azizi Ibrahim, Haslan Abu Hassana, Sabah M. Thahab, and Osama S Hamad. "The electrical properties of ZnO MSM Photodetector with Pt Contact Electrodes on PPC Plastic." *Journal of Electron Devic*es, vol. 7, pp. 225-229, 2010.

[88] Fumiyasu Oba1, Minseok Choi1, Atsushi Togo1 and Isao Tanaka1,2 "Point defects in ZnO: an approach from first principles." *Sci. Technol. Adv. Mater.,* vol. 12, 034302, 2011

[89] Lukas Schmidt-Mende and Judith L. MacManus-Driscoll. "ZnO – nanostructures, defects, and devices." *Materialstoday*, vol. 10, no. 5, pp.40-48.

[90] Anderson Janotti and Chris G. Van de Walle. "Native point defects in ZnO." *Pysical Review B,* vol. 76, 165202, 2007.

[91] M. D. McCluskey and S. J. Jokela. "Defects in ZnO." *J. Appl. Phys.,* vol. 106, 071101, 2009.

[92] Leonid V. Zhigilei. "Crystal Defects." University of Virginia, Charlottesville, VA, United States.

APPENDIX A SIMMON'S MODEL

The general formula of the tunneling current between electrodes separated by thin insulating film is derived by Simmon.

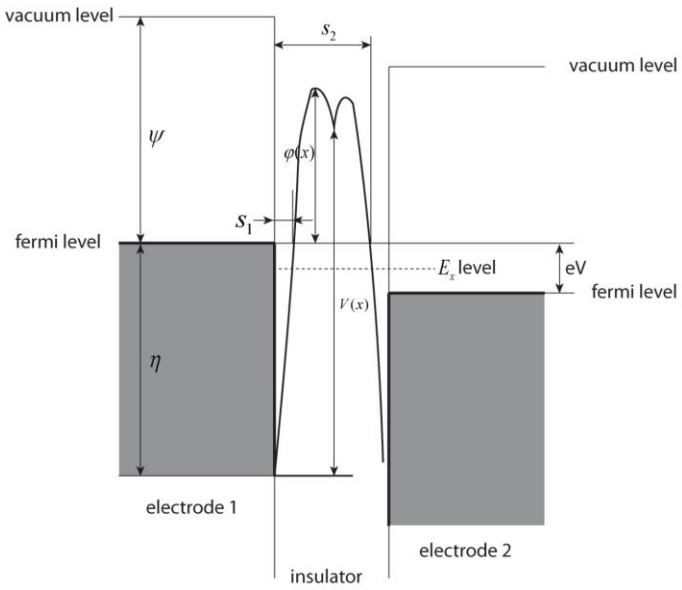

Figure A-1. General barrier in insulating film between two metal electrodes.

As can be seen in Figure A-1, the probability $D(E_x)$ that an electron can penetrate a potential barrier with barrier height $V(x)$ can be given by the WBK approximation:

$$D(E_x) = \exp\{-\frac{4\pi}{h}\int_{s_1}^{s_2}\sqrt{2m(V(x)-E_x)}dx\},$$

where s_1 ,s_2 are the limits of barrier at Fermi level, and $E_x = \frac{1}{2}mv_x^2$ is the energy component of the incident electron in the x direction. Number of electrons tunneling through the barrier from electrode 1 to electrode 2 is given by:

$$N_1 = \int_0^{v_m} v_x n(v_x) D(E_x) dv_x = \frac{1}{m} \int_0^{E_m} n(v_x) D(E_x) dE_x ,$$

where $n(v_x)dv_x$ is the number of electrons with velocity between v_x and $v_x + dv_x$ in unit volume and E_m is the maximum energy of the electrons in the electrode. The number of electrons with velocity between the usual infinitesimal limits in unit volume is given by:

$$n(v_x) = \frac{2m^3}{h^3} \int\int_{-\infty}^{+\infty} f(E) dv_y dv_z ,$$

where $f(E)$ is the Fermi-Dirac distribution function. Substituting the polar coordinates $E_r = \frac{1}{2} m v_r^{\,2}$ and $v_r^{\,2} = v_y^{\,2} + v_z^{\,2}$, we will have:

$$N_1 = \frac{4\pi m}{h^3} \int_0^{E_m} D(E_x) dE_x \int_0^{\infty} f(E) dE_r .$$

In a similar manner, the number of electrons tunneling through the barrier from electrode 2 to electrode 1 is given by:

$$N_2 = \frac{4\pi m}{h^3} \int_0^{E_m} D(E_x) dE_x \int_0^{\infty} f(E + eV) dE_r ,$$

where *V* is the voltage across film, *e* is the electron charge, and *h* is Plank's constant. The net flow of electrons through the barrier is

$$N = N_1 - N_2 = \int_0^{E_m} D(E_x) dE_x \times \{ \frac{4\pi m}{h^3} \int_0^{\infty} [f(E) - f(E + eV) .$$

Writing $\zeta_1 = \frac{4\pi me}{h^3} \int_0^{\infty} f(E) dE_r$ and $\zeta_2 = \frac{4\pi me}{h^3} \int_0^{\infty} f(E + eV) dE_r$, the above equation becomes

$$J = \int_0^{E_m} D(E_x) dE_x \times \{ \frac{4\pi me}{h^3} \int_0^{\infty} [f(E) - f(E + eV)] dE_r \} = \int_0^{E_m} D(E_x) \zeta dE_x ,$$

where $\zeta = \zeta_1 - \zeta_2$.

With $V(x) = \eta + \varphi(x)$, where η is the Fermi level of the electrode and $\varphi(x)$ is the barrier height, the probability becomes

$$D(E_x) = \exp\{-\frac{4\pi}{h}\sqrt{2m}\int_{s_1}^{s_2}\sqrt{\eta + \varphi(x) - E_x}\,dx\}.$$

It can be proved that $\int_{s_1}^{s_2}\sqrt{f(x)}dx \cong \beta\overline{f}\Delta s$, where $\beta = 1 - \frac{1}{8\overline{f}^2\Delta s}\int_{s_1}^{s_2}[f(x) - \overline{f}]^2 dx$. So we will have:

$$D(E_x) \approx \exp[-A\sqrt{\eta + \overline{\varphi} - E_x}],$$

where $\overline{\varphi} = \frac{1}{\Delta s}\int_{s_1}^{s_2}\varphi(x)dx$ is the mean barrier height above the Fermi level of the electrode that is negatively biased and $A = \frac{4\pi\beta\Delta s}{h}\sqrt{2m}$ with $\Delta s = s_2 - s_1$.

At 0 K, ζ_1 and ζ_2 are given by $\zeta_1 = \frac{4\pi me}{h^3}(\eta - E_x)$ and $\zeta_2 = \frac{4\pi me}{h^3}(\eta - E_x - eV)$.

Hence,

$$\zeta = \begin{cases} 4\pi me/h^3 * eV & 0 < E_x < \eta - eV \\ 4\pi me/h^3 * (\eta - E_x) & \eta - eV < E_x < \eta \\ 0 & E_x > \eta \end{cases}$$

Substituting the above equation in the current density equation gives:

$$J = \frac{4\pi me}{h^3}\left\{eV\int_0^{\eta - eV}\exp[-A\sqrt{\eta + \overline{\varphi} - E_x}]dE_x + \int_{\eta - eV}^{\eta}(\eta - E_x)\exp[-A\sqrt{\eta + \overline{\varphi} - E_x}]dE_x\right\}$$

It can be written as

$$J = \frac{4\pi me}{h^3}\left\{eV\int_0^{\eta - eV}\exp[-A\sqrt{\eta + \overline{\varphi} - E_x}]dE_x - \overline{\varphi}\int_{\eta - eV}^{\eta}\exp[-A\sqrt{\eta + \overline{\varphi} - E_x}]dE_x + \int_{\eta - eV}^{\eta}(\eta - E_x + \overline{\varphi})\exp[-A\sqrt{\eta + \overline{\varphi} - E_x}]dE_x\right\}.$$

The first integral yields

$$(\frac{8\pi me^2}{h^3A^2})V(A\sqrt{\bar{\varphi}+eV}+1)\exp(-A\sqrt{\bar{\varphi}+eV}).$$

The second integral yields

$$-(\frac{8\pi me}{h^3A^2})\bar{\varphi}[(A\sqrt{\bar{\varphi}}+1)\exp(-A\sqrt{\bar{\varphi}})-(A\sqrt{\bar{\varphi}+eV}+1)\exp(-A\sqrt{\bar{\varphi}+eV})].$$

The third integral yields

$$(\frac{8\pi me}{h^3A})[\bar{\varphi}^{\frac{3}{2}}\exp(-A\sqrt{\bar{\varphi}})-(\bar{\varphi}+eV)^{\frac{3}{2}}\exp(-A\sqrt{\bar{\varphi}+eV})]+(\frac{8\pi me}{h^3A})(\frac{3}{A})[\bar{\varphi}\exp(-A\sqrt{\bar{\varphi}})-(\bar{\varphi}+eV)\exp(-A\sqrt{\bar{\varphi}+eV})]\cdot$$

Summing these three equations, we will have:

$$J = J_0[\bar{\varphi}\exp(-A\sqrt{\bar{\varphi}})-(\bar{\varphi}+eV)\exp(-A\sqrt{\bar{\varphi}+eV})],$$

where $J_0 = \frac{e}{2\pi h}(\frac{1}{\beta\Delta s})^2$.

For very low voltage, since $eV \approx 0$ and $\bar{\varphi} >> eV$, above equation becomes

$$J = J_0[\bar{\varphi}-(\bar{\varphi}+eV)\exp(-\frac{AeV}{2\sqrt{\bar{\varphi}}})]\times\exp(-A\sqrt{\bar{\varphi}}) \approx J_L\sqrt{\bar{\varphi}}V\exp(-A\sqrt{\bar{\varphi}})$$

where $J_L = \frac{\sqrt{2m}}{\beta\Delta s}(\frac{e}{h})^2$.

Consider a rectangular barrier. As can be seen in Figure A-2, for low voltage range ($V \approx 0$), $\Delta s = s$, $\bar{\varphi} = \varphi_0$, and $\beta \approx 1$. Substituting these values gives:

$$J = \frac{\sqrt{2m\varphi_0}}{s}(\frac{e}{h})^2 V\exp(-\frac{4\pi s}{h}\sqrt{2m\varphi_0}).$$

For intermediate voltage range ($V < \varphi_0 / e$), $\Delta s = s$, $\bar{\varphi} = \varphi_0 - \frac{1}{2}eV$, and

$\beta = 1-\frac{(eV)^2}{96}(\varphi_0+\eta-E_x-\frac{eV}{2})^2 \approx 1$. The current density becomes

$$J = \frac{e}{2\pi hs^2}[(\varphi_0-\frac{1}{2}eV)\exp(-\frac{4\pi s\sqrt{2m}}{h}\sqrt{\varphi_0-\frac{1}{2}eV})-(\varphi_0+\frac{1}{2}eV)\exp(-\frac{4\pi s\sqrt{2m}}{h}\sqrt{\varphi_0+\frac{1}{2}eV})]\cdot$$

For high voltage range, $\Delta s = s\varphi_0 / eV$, $\bar{\varphi} = \frac{\varphi_0}{2}$ and

$\beta = 1 - \frac{(eV/s)^2}{8\Delta s} \frac{1}{(\varphi_0/2)^2} \int_0^{\Delta s} (\frac{1}{2}\Delta s - x)^2 dx = \frac{23}{24}$. Hence,

$$J = \frac{2e^3 (\frac{F}{\beta})^2}{8\pi h \varphi_0} [\exp(-\frac{4\pi\beta}{eFh}\sqrt{m}\varphi_0^{\frac{3}{2}}) - (1+\frac{2eV}{\varphi_0})\exp(-\frac{4\pi\beta}{eFh}\sqrt{m}\varphi_0^{\frac{3}{2}}\sqrt{1+\frac{2eV}{\varphi_0}})].$$

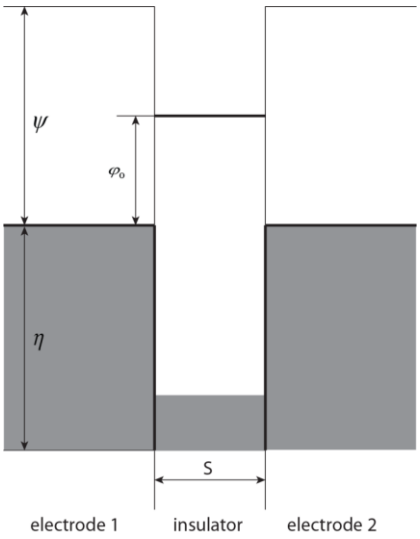

(a)

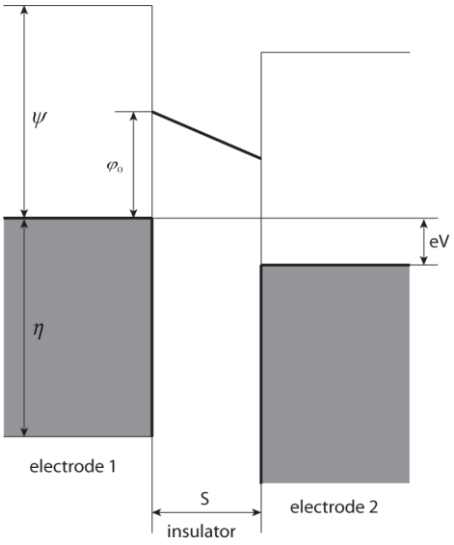

(b)

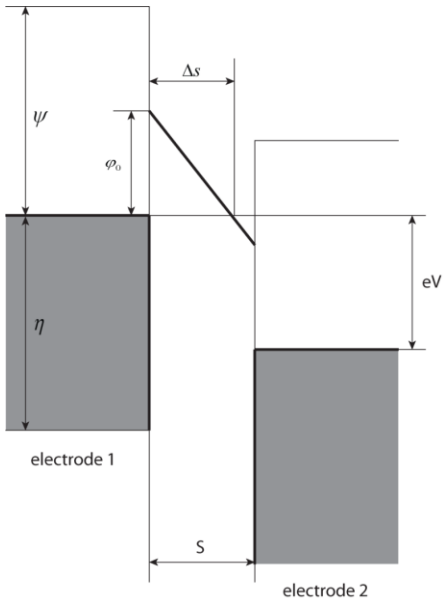

(c)

Figure A-2.Rectangular potential barrier in insulating film between metal electrodes for: (a) $V \approx 0$; (b) $V < \varphi_0 / e$; (c) $V > \varphi_0 / e$.

According to Simmon's model, if the size of the insulator, the potential barrier height, and the junction area are known, the current can be calculated with respect to the voltage applied.

Reference:

[1] John G. Simmons. "Generalized Formula for the Electric Tunnel Effect between Similar Electrodes Separated by a Thin Insulating Film." *J. Appl. Phys*. vol. 34, pp. 1793-1803, 1963.

APPENDIX B THE MATLAB PROGRAM TO CALCULATE THE SIZE OF THE NANOGAP

A MATLAB program has been made to plot the tunneling current based on Simmon's model. If the I-V curve of a device is measured, the size of the insulator between the electrodes can be estimated by fitting the data with the program. Therefore, the size of the nanogap can be obtained.

To check if the program can accurately calculate the tunneling current, the program has been used to plot the data of other researchers' work.

A junction formed by Al and AlO_x has been made by Schaefer et al. The junction has the area of $3*10^{-7}$ cm^2. The barrier height is 1.4 eV. The size of the barrier is 1.8 nm. Figure B-1 shows the I-V curve and the fittings of the Simmon's equation to the data presented in the paper. Figure B-2 is the plot of the I-V curve calculated by the MATLAB program in this thesis using the same parameters. As can be seen in the figures, the shape of the two plots and the current values are very similar.

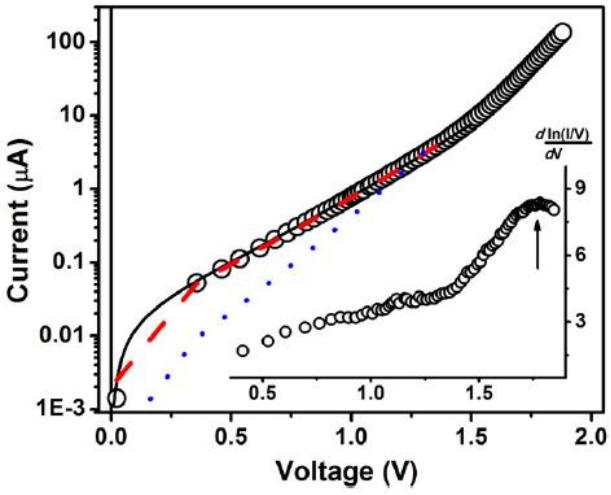

Figure B-1. I-V curve measured at room temperature and fittings of Simmons' equation of the AlO_x tunneling barrier.

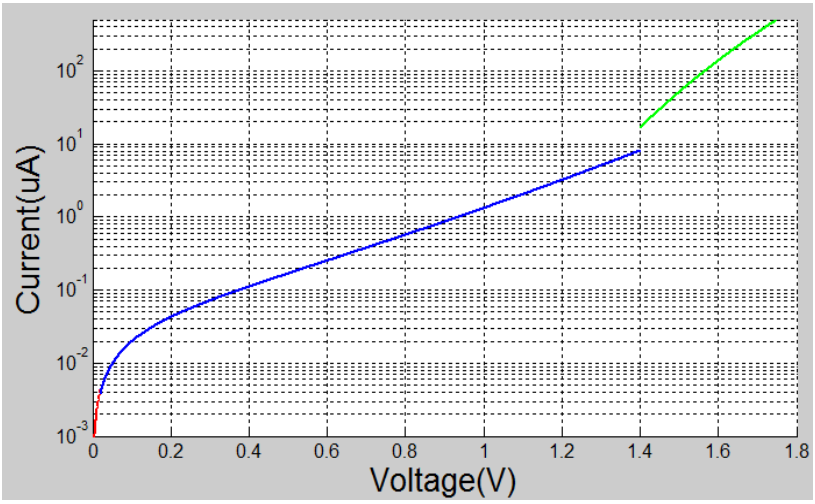

Figure B-2. I-V curve of the AlO_x tunneling barrier plotted by the MATLAB program.

Fan et al. have fabricated a tantalum (Ta) granular oxide-metal junction. The barrier height is 0.56 eV. The junction has the area of 15 nm^2. The size of the barrier is 1.787 nm. Figure B-3 shows the experimental and calculated I-V curve of the junction presented in the paper. Figure B-4 is the I-V curve plotted by the MATLAB program using the same parameters. The plot in the Figure B-4 is very close to the experimental data in Figure B-3 in the low voltage range.

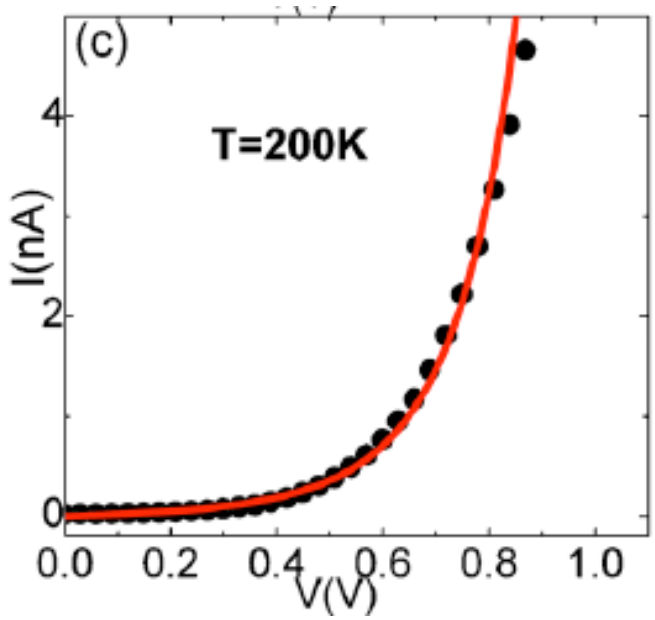

Figure B-3. The experimental and calculated I-V curve of the Ta oxide-metal junction.

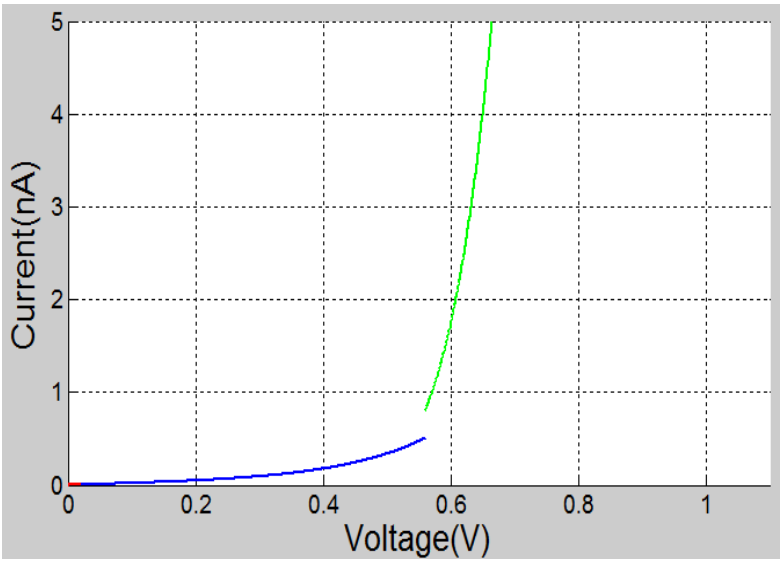

Figure B-4. I-V curve of the Ta oxide- metal junction calculated by the MATLAB program.

Based on the comparison of the experimental data and the calculated I-V curve plotted by the MATLAB program, it can be concluded that the program can work

effectively to plot the I-V curve of a metal-insulator-metal junction and the size of between the metal electrodes can be estimated as well.

Reference:

[1] D M Schaefer, P F P Fichtner, M Carara, L F Schelp, and L S Dorneles. “Dielectric breakdown in AlOx tunnelling barriers.” *J. Phys. D: Appl. Phys.*, vol. 44, no. 13, 135403, 2011.

[2] Wenbin Fan, Jiwei Lu, and Stuart A. Wolf. “Electron conduction in lateral granular oxide-metal tunnel junctions.” Appl. Phys. Lett., vol. 97, no. 24, 242113, 2010.

APPENDIX C THE CODES OF THE MATLAB PROGRAM

```
clear all;
syms a b c d f g e h s  V1 V2 V3 phi beta m  J1 J2 J3 a b c d;
e = 1.6*10^(-19);  %C electron charge%
h = 6.63*10^(-34);  %J/s planks constant%
phi = (1.4)*1.6*10^(-19);  %J barrier height%
s = 1.8*10^(-9);  %m gap size%
m = 9.11*10^(-31);  %kg electron mass%
beta = 23/24;
A = 3*10^(-7)*10^(-4);%m^2 junction area%
V1 = 0:0.001:0.02;      %V low voltage range%
V2 = 0.02:0.001:1.4; %V medium voltage range%
V3 = 1.4:0.001:1.8;      %V high voltage range%

a = e/(2*pi*h*s^2);
b = -4*pi*s/h;
c = sqrt(2*m*(phi-e*V2/2));
d = sqrt(2*m*(phi+e*V2/2));
f = e^3/(4*pi*h*phi*s^2*beta^2);
g = -4*pi*beta/e/h*m^(1/2)*phi^(3/2);

J1= sqrt(2*m*phi)/s*(e/h)^2*V1*exp(b*sqrt(2*m*phi)); % current density - low voltage%
J2 = a*((phi-e*V2/2).*exp(b*c)-(phi+e*V2/2).*exp(b*d)); % current density - medium
voltage%
J3 = f*(exp(g*s./V3)-(1+2*e*V3/phi)*exp(g*s*sqrt(1+2*e*V3/phi)/V3)).*V3.^2; %
current density - high voltage%

I1 = J1*A; %  current- low voltage%
I2 = J2*A; %  current - medium voltage%
I3 = J3*A; % current - high voltage%

labelFontSize = 20;
numberFontSize = 20;
markerSize = 2;
lineWidth = 2;

hold on;

plot(V1,I1,'r.-','LineWidth',lineWidth,...
          'MarkerSize',markerSize),grid on; % I-V  low voltage%
plot(V2,I2,'b.-','LineWidth',lineWidth,...
          'MarkerSize',markerSize),grid on; % I-V  medium voltage%
plot(V3,I3,'g.-','LineWidth',lineWidth,...
         'MarkerSize',markerSize),grid on; % I-V  high voltage%
```